Is the SMC Bound to the LMC? The *HST* Proper Motion of the SMC

Nitya Kallivayalil[1]

Harvard-Smithsonian Center for Astrophysics, 60 Garden Street, Cambridge, MA 02138

Roeland P. van der Marel[2]

Space Telescope Science Institute, 3700 San Martin Drive, Baltimore, MD 21218

Charles Alcock[3]

Harvard-Smithsonian Center for Astrophysics, 60 Garden Street, Cambridge, MA 02138

ABSTRACT

We present a measurement of the systemic proper motion of the Small Magellanic Cloud (SMC) made using the Advanced Camera for Surveys (ACS) on the *Hubble Space Telescope* (*HST*). We tracked the SMC's motion relative to 4 background QSOs over a baseline of approximately 2 years. The measured proper motion is : $\mu_W = -1.16 \pm 0.18$ mas yr^{-1} , $\mu_N = -1.17 \pm 0.18$ mas yr^{-1} . This is the best measurement yet of the SMC's proper motion. We combine this new result with our prior estimate of the proper motion of the Large Magellanic Cloud (LMC) from the same observing program to investigate the orbital evolution of both Clouds over the past 9 Gyr. The current relative velocity between the Clouds is 105 ± 42 km s^{-1} . Our investigations of the past orbital motions of the Clouds in a simple model for the dark halo of the Milky Way imply that the Clouds could be unbound from each other. However, our data are also consistent with orbits in which the Clouds have been bound to each other for approximately a Hubble time. Smaller proper motion errors and better understanding of the LMC and SMC masses would be required to constrain their past orbital history and their bound vs. unbound nature unambiguously. The new proper motion measurements should be sufficient to allow the construction of improved models for the origin and properties of the Magellanic Stream. In turn, this will provide new constraints on the properties of the Milky Way dark halo.

[1]nkalliva@cfa.harvard.edu

[2]marel@stsci.edu

[3]calcock@cfa.harvard.edu

Subject headings: galaxies: kinematics and dynamics – galaxies: interactions – Magellanic Clouds

1. Introduction

The Large and Small Magellanic Clouds (LMC & SMC), both satellites of the Milky Way (MW), provide a unique opportunity to study interacting galaxy pairs and three-body systems. It is expected from current models of hierarchical structure formation (e.g. Zentner & Bullock 2003) that the interaction between the Clouds and the MW will have played an important role in the dynamical evolution of the MW's outer parts (e.g. Font et al. 2006). A resonant interaction between the LMC & the MW is thought to be responsible for the MW warp (Weinberg & Blitz 2006). In return, the MW has had a major influence on the Clouds' development, including their star formation history (Holtzman et al. 1997; Harris & Zaritsky 2001; Smecker-Hane et al. 2002), structural and chemical evolution (Mathewson et al. 1986; Bekki & Chiba 2005), and kinematics (Hatzidimitriou et al. 1993; Cole et al. 2005). This three-body interaction is also linked to the origin of the Magellanic Stream, an approximately circum-polar HI feature that trails the Clouds in their orbit around the MW (Wannier & Wrixon, 1972; Mathewson et al. 1974; Putman et al. 1998), the inter-Cloud bridge (Putman et al. 1998), and the complicated geometry (Caldwell & Coulson 1986; Crowl et al. 2001; but see also Welch et al. 1987) and gas distribution of both Clouds (Stanimirović et al. 2004; Gardiner et al. 1994). Some current dwarf galaxies and globular clusters may have originated from tidal stripping as the Clouds orbited the Galaxy (Lin et al. 1995).

The Magellanic Stream and any stars that have been tidally stripped from the Clouds as they orbit the MW provide a "fossil record" of the history of the build-up of MW mass (e.g. Belokurov et al. 2006; Peñarrubia et al. 2005; Johnston et al. 1999). Decoding this record requires detailed modeling, describing how the internal evolution of the satellites is affected by tides, and sensitive observations that make it possible to falsify theoretical predictions. A major uncertainty in this effort is the orbital motion of the Clouds. While the radial velocities of the Clouds have been measured to high precision (van der Marel et al. 2002; Harris & Zaritsky 2006), the velocity transverse to the line of sight (the proper motion) has been harder to constrain. This uncertainty complicates the efforts to infer the fossil record because the past history of the Clouds is ambiguous.

There have been several groups involved in modeling the orbits of the Clouds around the Galaxy with the intent of reproducing the Magellanic Stream (Murai & Fujimoto 1980; Lin & Lynden-Bell 1982; Heller & Rohlfs 1994; Moore & Davis 1994; Lin et al. 1995; Gardiner & Noguchi 1996; Yoshizawa & Noguchi 2003; Mastropietro et al. 2005; Connors et al. 2005).

The models fall into two main categories: tidal models and ram-pressure stripping models. The former deal with the tidal force exerted by the Galaxy on the MCs. The Stream is modeled as a product of the tidal disruption of the SMC, and the inter-Cloud region is the result of a close encounter between the Clouds, which are assumed to have been a bound system for the past Hubble time. In general, the conclusions of these studies are that the MCs are near perigalacticon, they are gravitationally bound to the Galaxy with apogalacticon beyond 100 kpc, and it is expected that they will become separated in the next 1 - 2 Gyr. The gas in the Stream is thought to have originated from the SMC between 1 - 2 Gyr ago, and the mass in the Stream is comparable to the gas content in the SMC itself (Lin et al. 1995, Putman et al. 2003).

The ram-pressure models also invoke an encounter between the Clouds to produce the inter-Cloud region, and subsequently the Stream is produced from collisions between the inter-Cloud region gas and either high velocity clouds in the Galactic halo ('discrete ram-pressure stripping'; Wayte 1991) or an extended halo of diffuse ionized gas ('diffuse ram-pressure stripping'; Moore & Davis 1994). The ram-pressure stripping models have some difficulty in producing the leading arm of the Stream, while the tidal models do so naturally (Connors et al. 2005). Also, the number density of high velocity clouds in the outer halo is uncertain, as is the existence of a sufficiently dense extended gaseous halo. The ram-pressure stripping models have become quite sophisticated (Mastropietro et al. 2005), but so far only include the LMC in the analysis and not the SMC. The tidal models too, while increasingly detailed, have a few open questions which might only be adequately addressed with the inclusion of more detailed gas-dynamical properties. For instance, the lack of symmetry between the leading and trailing arms of the Stream are indicative of drag on the HI gas, and the apparent lack of stars in the Stream is still poorly understood. While there is some evidence for tidally stripped Magellanic stars far (22°) from the LMC center and in the direction of the Carina dwarf (Muñoz et al. 2006), no stars have yet been associated with the Magellanic Stream itself.

If the space velocities of both Clouds were known accurately enough they would be a valuable tool in understanding evolutionary features of both the Clouds and the MW. As stated above, the radial velocities of the Clouds have been more readily determined than the transverse velocities, which can only be estimated via proper motions. Since the LMC is closer and larger, there has been much more detailed work on its proper motion. There is now good general agreement between the results from various teams (see Kallivayalil et al. 2006; hereafter Paper I). But it is worth noting that while the implied LMC space velocities agree with some of the models of the Stream (Heller & Rohlfs 1994), they differ by ~ 100 km s^{-1} from others (Gardiner & Noguchi 1996). The proper motion of the SMC, has been much harder to constrain. A good inertial reference frame for such a measurement has been hard

to come by. CCD astrometry with a good sample of background QSOs is necessary to get a handle on its proper motion.

Previous work on the SMC proper motion includes: Kroupa & Bastian (1997) who used Hipparcos measurements of 11 stars to get $\mu_W = -1.23 \pm 0.84, \mu_N = -1.21 \pm 0.75$ mas yr^{-1} (here we define the proper motions μ_W, μ_N in the directions west and north as $\mu_W \equiv -\mu_\alpha \cos(\delta)$ and $\mu_N \equiv \mu_\delta$). There is also a study by Irwin et al. (1996) using AAT (Anglo-Australian Telescope) and CTIO (Cerro Tololo Inter-American Observatory) 4m photographic plates covering a baseline of 15 - 20 years. A measurement of $\mu_W = -0.92 \pm 0.2$, $\mu_N = -0.69 \pm 0.2$ mas yr^{-1} is quoted in Irwin (1999), but the analysis of these data is unpublished. Anderson & King (2004b) measured a very accurate relative proper motion between the SMC and the Globular Cluster 47 *Tucanae* of $\Delta\mu_W = -4.716 \pm 0.035$ mas yr^{-1} and $\Delta\mu_N = -1.357 \pm 0.021$ mas yr^{-1} . When combined with an estimate of the absolute proper motion of 47 *Tucanae* by Freire et al. (2003), who report $\mu_W = -5.3 \pm 0.6$ mas yr^{-1} and $\mu_N = -3.3 \pm 0.6$ mas yr^{-1}, this implies that the SMC's proper motion is $\mu_W = -0.6 \pm 0.6$ mas yr^{-1}, $\mu_N = -1.9 \pm 0.6$ mas yr^{-1} . The unweighted average of these three independent SMC proper motion measurements[1] is $\langle \mu_W \rangle = -0.91 \pm 0.19$ mas yr^{-1} , $\langle \mu_N \rangle = -1.28 \pm 0.36$ mas yr^{-1} . This is broadly consistent with the current understanding of the Magellanic Stream and the MC-MW system, but the errors are are not accurate enough to significantly constrain its dynamics.

In this paper, we present the results of a project that has allowed us to measure the systemic proper motion of the SMC to 15% accuracy using *HST* observations of a sample of background QSOs, with just a two year baseline. Our results for the LMC from the same *HST* program were presented in Paper I. § 2 describes the QSO sample; § 3 summarizes the analysis of the data; § 4 presents the SMC proper motion results. We then move on to an investigation of the global dynamics of both the LMC and the SMC given our new velocity measurements. § 5 describes the Clouds' movements within a fiducial model of the Galactic halo and § 6 gives a discussion and summary of the results.

---

[1]Momany & Zaggia (2005) recently obtained a very different proper motion for the SMC using the USNO CCD Astrograph all-sky Catalog (UCAC2) : $\mu_W = -4.44$ mas yr^{-1} ; $\mu_N = -2.94$ mas yr^{-1} . This is inconsistent with our current knowledge of the MC-MW system and probably indicates the presence of systematic errors in the catalog, as the authors themselves point out. We therefore ignore this measurement in the following.

2. Sample

Geha et al. (2003) identified 10 QSOs behind the SMC from their optical variability in the MACHO database. We proposed to image all 10 fields using snapshot mode with the High Resolution Camera (HRC) on the Advanced Camera for Surveys (ACS) on *HST*. In snapshot mode every target is not guaranteed, but rather, observations are taken throughout the cycle, whenever they can be fit in, according to manually assigned priorities. In the first epoch snapshot program (Cycle 11; GO 9462) we successfully imaged the fields around 6 of the 10 SMC QSOs. This is a typical completion rate for snapshot programs. In the second epoch (Cycle 13; GO 10130) we successfully imaged 5 out of the 6 proposed SMC QSOs. The 5 QSOs are favorably placed behind the central few degrees of the SMC where we do not expect to be unduly influenced by any tidal features (see Kroupa & Bastian 1997). Figure 1 shows the sample of QSOs behind the SMC. White circles represent the 5 QSOs for which we did get 2 epochs of HRC data and white squares mark the QSOs for which we did not. Table 1 lists the QSO ID, the MACHO ID (for reference with Geha et al. 2003), the RA, DEC (J2000), V-magnitude and redshift for each of the 5 QSOs.

Our observational strategy is described in detail in Paper I and the reader is referred to it for the specifics. The SMC QSOs were part of the same dataset as the LMC QSOs and the data were taken in an identical fashion. The HRC was chosen for its high resolution, the fact that it is well sampled, well calibrated, and that its higher order distortion has been understood and characterized (Anderson & King 2004a; Krist 2003). Our observing strategy was to use many short-exposure, dithered V-band images for the astrometry. In the first epoch, we imaged each QSO field with the F606W filter (broad V) using two four-point dither patterns that were shifted relatively by 8 integer pixels (8 frames in total; see Figure 3 in Paper I for a schematic of the dither pattern.). Each field was also imaged with the F814W filter (broad I) using a simple CR-SPLIT. In epoch 2 we implemented the same F606W sequence, but did not re-do the F814W observations, since we could use the existing first epoch I-band images for any non-astrometric purposes. Table 1 lists the date of observation and exposure times for each filter for each epoch. The average baseline achieved is ~ 2 years.

One important potential source of systematic error in these measurements arises from the relative orientation of the focal plane at the two epochs. For observations with *HST*, the date of observation determines the orientation of the detector axes with respect to the sky. In the case of Paper I we were in the happy situation that we had many QSO fields all of which were observed at random times of the year with random roll angles of the telescope. The fact that our LMC observations were all carried out at different times and with different orientations allowed any systematic errors that were tied to the CCD frame to average out as $\sim 1/\sqrt{N}$. We are not so fortunate with the SMC fields however, because there are far

fewer of them, and because three of them (S1, S2 & S3) were observed at about the same time and hence at very similar roll angles. Table 1 lists the dates of observation in each epoch and the value of ORIENTAT, which is the position angle on the sky of the detector y-axis, for each of the 5 SMC fields. So if there are systematic errors that are tied to the CCD frame then they would not have averaged out to the same extent as for the LMC data. § 3.2 will discuss the possibility of systematic errors in detail.

3. Analysis

3.1. Procedure to Obtain a Proper Motion from Each QSO field

We followed the same procedure to analyze the SMC QSO fields as in Paper I (see Figure 4 of Paper I). We will only summarize our method here and the interested reader should look to Paper I for a detailed explanation. We used Anderson & King (2004a; hereafter AK04) software to fit a filter-dependent point-spread function (PSF) to the flat-fielded images (_flt.fits) from the STScI pipeline, and to geometrically correct the raw positions and fluxes of point sources on the detector chip to account for the higher-order distortion on the ACS. The geometric distortion is very well understood and has been characterized by Anderson & King (AK04) to ~ 0.005 pixels. We then created a master-list of sources for each QSO field by cross-referencing all 18 frames (16 V-band and 2 I-band) with the first V-band frame from the first epoch (our 'reference' image). In this way, the master-list only contained sources that were present in all 18 frames. We then used a six-parameter linear fit to bring the star-field of each of the 16 V-band frames into alignment with the reference frame. This fit accounts for a rotation, a translation, for scale changes and for skew terms (which account for non-orthogonality between the two detector axes). These linear transformations are needed to account for the translational dithering of the observations, the difference in telescope orientation between epochs, and the effects of "breathing" and differential velocity aberration (AK04). The linear fit also accounts to lowest order for the charge-transfer efficiency (CTE) degradation of the telescope (this is a linear effect with position on the y-axis, although in a strict sense it also depends on stellar brightness). The QSO was removed from the master-list before this fit was implemented.

Once we had a good working guess at the transformation, cuts were made in the proper motion (PM)- and proper motion error (δPM)-space of the stars in the field to ensure that foreground (Galactic) stars with large proper motions or stars with large centroiding errors were not used in the fit. A new six-parameter linear transformation was found for this star-list, and the process was iterated until the number of stars used in the fit was unchanging. Once the terms of the transformations had converged, the reflex motion of the QSO, i.e.

the difference between its average position in the two epochs, was measured with respect to the star-field using the final transformation. This is then $-1\times$(the PM of the SMC). The error in the SMC PM of each QSO field is estimated as the quadrature sum of the following two quantities: 1) the error in the PM of the QSO, which is the quadrature sum of the centroiding errors from each epoch, and 2) the error in the average PM (itself zero) of the star field. This latter quantity gives us an idea of our systematic errors by describing how accurately we were able to align the star fields between the two epochs. In order to estimate it, the PM of each star was determined as the difference between its average position in epoch 2 and epoch 1, and then the error in the average PM of all the stars was calculated.

3.2. Consistency Checks

Figure 2 is a $(V-I,\, V)$ CMD of our SMC fields. QSOs are shown in green, stars with PM and δPM < 0.1 pixels (the cut that we applied in PM and δPM space) are shown in red, and the remaining sources in the master-lists are shown in black. The CMD has the expected shape, with a clearly defined main sequence and giant branch. There are a small number of red clump stars at $\sim V = 19.5,\ V-I = 0.9$ (see Dolphin et al. 2001). This is, as expected, approximately half a magnitude fainter than what we found for the LMC and provides an additional calibration check. The QSOs appear spread out over the CMD as we saw in the case of the LMC. As in the LMC dataset, the QSOs behind the SMC are not systematically the brightest sources in the images nor do they all have the same color. This minimizes potential magnitude-based and color-based errors.

Figure 3 shows the final QSO PM errors ($\delta\mathrm{PM_{QSO}}$) versus the final error in the average motion of the star-field between epoch 1 and epoch 2 ($\sigma_{<\mathrm{PM}>}$). The average motion of the star-field itself was set up to be zero in our linear transformations and any deviation from zero is a signal of systematic errors. The plot shows that the final errors are dominated by the centroiding errors of the QSOs and that aligning the star-field introduces smaller errors in comparison. This is what we expected given that many stars were used to fit for the terms of the linear transformations.

Figures 4(a) & (b) show the PMs and δPMs of all the stars in the master-lists as a function of V magnitude. The plots have the expected $(S/N)^{-1}$ shape. The apparent discontinuity at ~ 0.1 pixels is a result of the cuts applied in the stars that were used to solve for the linear transformations. Figure 4(c) shows δPM versus PM for all the stars in the master-lists. It shows that the PM residuals for the stars are not much larger than the expected random errors. The next two figures seek to address the possibility of any systematic trends as a function of chip location. Figure 5 is a plot of the PMs of the stars

which have PM & δPM < 0.1 pixels versus x and y-position on the chip separately. There is no obvious trend with position on the chip and the scatter looks comparable in both x and y. Figure 6 is a plot of the average PM value for every 200 binned pixels in an effort to get down to the level of the noise. As can be seen from this plot, there is no evidence for systematic errors larger than ~ 0.005 pixels, which confirms the findings of AK04.

4. Results

4.1. Proper Motion Results for the SMC

Table 2 presents the results for each QSO field obtained using the procedure discussed in § 3.1. $N_{\rm sources}$ refers to the number of real sources in each field (present in at least half of the frames), $N_{\rm master}$ refers to the number of stars in the master-list, and $N_{\rm used}$ is the number of stars used in the final transformation after the iteration scheme had converged. Each observed QSO PM provides an independent estimate of the PM of the SMC center of mass. Having obtained these estimates, we are now in a position to check for any further systematic trends on a per-field basis.

Figure 7 is a plot of the residual PM ($\mu_{\rm resid}$) for each QSO field as a function of V magnitude, $V-I$ color, $N_{\rm used}$, $\chi^2/N_{\rm used}$ and distance of the QSO from its nearest neighbor star. The residual PM is measured with respect to our final PM estimate for the SMC (see equation (1)). An analogous plot in Paper 1 alerted us to systematic effects as a function of $N_{\rm used}$ and $\chi^2/N_{\rm used}$, and consequently, we made cuts in the LMC dataset which amounted to using only those fields with $N_{\rm used} > 16$ and $\chi^2/N_{\rm used} < 15$. We have made the same cuts in the current dataset. This eliminated one field, S4, that has a very low value of $N_{\rm used}$. S4 is a particularly sparse field located towards the North-West of the SMC (see Figure 1). It has a very discrepant PM (see Table 2) and is shown with an open circle in Figure 7. The remaining fields are shown with closed circles. The PM estimates for these remaining fields show no obvious systematic trends associated with any of the above quantities.

Figure 8 is a plot of the QSO PMs for the 4 remaining fields in the (μ_W, μ_N)-plane. They are shown in comparison to the proper motions of the SMC stars used in the analysis. The stars are shown with points and the QSOs with filled circles. The PMs of the stars cluster around zero as expected given their PM errors (see Figure 4 (a) & (b); the error bars are not shown here). The reflex motions of the QSOs are clearly distinguishable from the star motions. The solid lines mark our final value for the SMC PM presented in equation (1) and discussed below.

The four available measurements for the SMC PM agree very well, to within ± 0.04 mas yr^{-1},

in the North-South direction (see Table 2). However, in the East-West direction there is agreement only to ± 0.32 mas yr^{-1}, indicating the presence of unidentified systematic errors. This is not surprising in view of our results obtained for the LMC in the context of the same observing program. The RMS scatter of the proper motion measurements from each LMC field was larger than the scatter expected from random errors alone, indicating the presence of systematic errors in our LMC measurement as well.

For the LMC, after using the same rejection criteria in terms of $N_{\rm used}$ and $\chi^2/N_{\rm used}$ as we do here we were left with 13 measurements. We estimated the final proper motion as the weighted average of the $N = 13$ measurements. The error in the result was estimated as the RMS scatter divided by $\sqrt{N}$, as expected for an ensemble of independent and uncorrelated measurements. This was appropriate because the following three criteria were met: (1) the measurements were obtained for different fields, at different positions in the galaxy; (2) the observations were obtained at different times of the year, with the relative orientation between the North direction and the detector y-axis distributed more or less randomly; and (3) the scatter in the final proper motion residuals appeared to be distributed randomly.

The situation for the SMC is somewhat more complicated than for the LMC, because neither the second nor the third criteria in the previous paragraph appears to be met. Observations S1, S2 and S3 were obtained with very similar telescope orientation (to within $\pm 6^\circ$) in both epochs, while observation S5 used a very different orientation in the first epoch (see Table 1). Moreover, the proper motion results for S1, S2 and S3 are in excellent agreement with each other (to better than ± 0.1 mas yr^{-1} in both coordinates), while the result for S5 differs by 0.4–0.6 mas yr^{-1}. So it appears that the unknown systematic errors in the study are correlated with telescope orientation. This is not surprising because any uncertainties in the geometric distortion correction would have fixed orientation in the detector frame.

The proper motion results suggest that it would be a mistake to treat S1, S2, S3 and S5 as independent and uncorrelated measurements. That would underestimate the error bars on the final proper motion result. Instead, we first take the weighted average proper motion of S1, S2 and S3. This gives $(\mu_W, \mu_N) = (-0.89 \pm 0.05, -1.18 \pm 0.05$ mas yr^{-1}), where the listed errors account only for the propagation of random errors. We denote this measurement as S123, and treat this as one of only two independent measurements of the SMC proper motion (the other one being S5). This is conservative in that it increases the error bars on the final proper motion measurement.

In our LMC proper motion study we found that the scatter between the PM estimates obtained from different fields was larger than expected based on the random errors alone. This indicates that the true error for each field has not only a random component, but also a systematic component. The observed scatter implies a systematic error of 0.24 mas yr^{-1}

per coordinate per field. For the LMC this error could be estimated directly, because the large number of available fields allowed a reliable calculation of the scatter. This is not true for the SMC, because S123 and S5 provide only two independent measurements. However, the SMC and LMC data were obtained with the same setup, in the same observing program, and at the same general time. So it is reasonable to assume that the systematic errors for the LMC and SMC fields are the same. For both the S123 and S5 measurements we then calculate a total error by adding in quadrature a systematic error estimate of 0.24 mas yr^{-1} per coordinate (based on the LMC results) to the random errors. We then take the weighted average of S123 and S5 as our final estimate for the SMC proper motion. This yields

$$\mu_W = -1.16 \pm 0.18 \text{ mas yr}^{-1} \,,\ \mu_N = -1.17 \pm 0.18 \text{ mas yr}^{-1} \quad (HST). \tag{1}$$

where the errors now take into account both random and systematic errors. The final errors per coordinate are larger by a factor 2.8 than what we obtained in our LMC proper motion study. This is plausible, since one would naively expect the errors to scale as the inverse square root of the number of measurements; and for comparison $\sqrt{13/2} = 2.5$.

Figure 9 is a vector plot of the residuals between the PM estimates for each field and the adopted average (equation (1)), shown with the 1σ error bars for each field. Circles show the positions of the QSO fields in RA/DEC space. Closed circles represent the final 4 fields that were used in our final estimate for the PM and the open circle shows the rejected field S4. The thick vector anchored by a plus sign shows the size of the inferred center of mass proper motion of the SMC at the adopted SMC center. The vectors appear to be randomly oriented in the sky. In particular, there is no evidence for any residual rotation of the SMC. We discuss the rotation of the SMC in more detail in § 4.2 below.

Our measurement of the SMC proper motion agrees to within 1σ with the one obtained in § 1 as the unweighted average of the three existing measurements, $\langle\mu_W\rangle = -0.91 \pm 0.19$ mas yr^{-1} , $\langle\mu_N\rangle = -1.28 \pm 0.36$ mas yr^{-1} . However, our result has either smaller errors or better understood errors than all previous work. The weighted average of our result with the quoted $\langle\mu_W\rangle, \langle\mu_N\rangle$ is :

$$\mu_W = -1.04 \pm 0.13 \text{ mas yr}^{-1} \,,\ \mu_N = -1.19 \pm 0.16 \text{ mas yr}^{-1} \quad (\text{HST} + \text{other studies}). \tag{2}$$

We show our HST measurement together with previous measurements in Figure 10, along with the corresponding 68.3% confidence ellipses. In the discussion that follows we adopt the HST-only values given in equation (1).

4.2. Three-Dimensional Space Motion of the SMC

The proper motion of the SMC gives the following values for the x and y components of the SMC velocity in a Cartesian system on the sky, with x in the direction of west and y in the direction of north:

$$(v_x,\ v_y) = (-340 \pm 52, -341 \pm 53)\ \mathrm{km\ s^{-1}}\ , \tag{3}$$

assuming a distance modulus of 18.95 (Cioni et al. 2000 and references therein). The corresponding transverse velocity, v_t, is 481 km s^{-1} at a position angle, $\Theta_t = 135°$. These can be combined with the observed line-of-sight velocity, 146 ± 0.6 km s^{-1} (Harris & Zaritsky 2006), and corrected for the reflex motion of the Sun, to give the full three-dimensional space velocity in a Galactocentric rest frame. The latter consists of a Cartesian coordinate system (X, Y, Z) with the origin at the Galactic center, the Z-axis pointing toward the Galactic north pole, the X-axis pointing in the direction from the Sun to the Galactic center, and the Y-axis pointing in the direction of the Sun's Galactic rotation. Following the procedure outlined in §9.2 of van der Marel et al. (2002) we get:

$$\begin{aligned} \mathbf{v}_{\rm SMC} &= (-87 \pm 48,\ -247 \pm 42,\ 149 \pm 37)\ \mathrm{km\ s^{-1}}\ , \\ v_{\rm SMC} &= 302 \pm 52\ \mathrm{km\ s^{-1}}\ , \\ v_{\rm SMC,rad} &= 23 \pm 7\ \mathrm{km\ s^{-1}}\ , \\ v_{\rm SMC,tan} &= 301 \pm 52\ \mathrm{km\ s^{-1}}\ , \end{aligned} \tag{4}$$

for the three-dimensional velocity of the SMC and its radial and tangential components. The LMC and SMC space velocities are summarized in Table 3.

We do not model any internal rotation contributions to the center of mass motion of the SMC. This is because a spectroscopic analysis of the radial velocities of 2046 red giants in the SMC by Harris & Zaritsky (2006) indicates that the SMC has no intrinsic rotation. These authors find a small velocity gradient across the SMC of 8.3 km s^{-1} deg^{-1} and argue that the origin of such a gradient need not be internal rotation but could instead be due to the differential projection of the SMC's tangential velocity along different lines of sight. They calculate that a tangential motion of ~ 500 km s^{-1}, which is close to the value that we measure in this work, will result in an apparent velocity gradient of 8.7 km s^{-1} deg^{-1} over the face of the SMC. They argue that even if the SMC has some small intrinsic rotation, its value is much smaller than the velocity dispersion that they measure ($\sigma = 27.5$ km s^{-1}), and thus that the SMC is primarily supported by its velocity dispersion. By contrast, the HI gas in the SMC does show clear rotation (Stanimirovic et al. 2004). This presumably indicates that the HI gas resides in a more disk-like distribution than the stars. Even if the stars in the SMC were to rotate as fast as the gas (which appears ruled out by the Harris & Zaritsky

2006 observations), then this still would not significantly affect our results. At the position of our QSO fields, the component of the HI rotation velocity field projected onto the plane of the sky amounts to a proper motion of only ~ 0.09 mas yr^{-1} . This is within the error bars of our final result. Moreover, our result is obtained as an average of different fields. If there were rotation of the SMC stars, then the rotation velocity vectors for the different fields would not align on the sky. Hence, they would partially cancel out when averaged.

5. The Orbits of the Clouds around the Milky Way

5.1. The Fiducial Model

We are now in a position to ask how the orbits of the two Clouds have evolved over the past several giga-years (Gyr). Using the six position and six velocity components of both Clouds as initial conditions we can obtain a solution for the Clouds' movements in a prescribed dark halo model. As a fiducial model we use a scheme that has been used many times before in the literature and was originally formulated by Murai & Fujimoto (1980; see also Gardiner et al. 1994; Gardiner & Noguchi 1996; Bekki & Chiba 2005), albeit in the absence of tangential velocity information, especially for the SMC.

In order to derive the orbits of the Clouds, we first need the current tangential velocities (from this study), line of sight velocities and three-dimensional position parameters (from the literature). A summary of the orbital parameters that we use is given in Table 3. In addition to the current phase-space parameters, we need to assume models or values for the following: the gravitational potential of the Galaxy, the gravitational potential of the Clouds, the total masses and mass profiles of the Clouds, the dynamical friction between the Clouds and the Galactic halo, and that between the Clouds themselves. So there is a large number of physical assumptions and parameterizations necessary to calculate orbits. There has been much progress in the arena of galaxy models (Hernquist 1990; Navarro, Frenk & White 1997), and there might be reason to deviate significantly from prior approaches. However, the goal in the present paper is merely to see what we obtain for the orbital evolution of the Clouds when we combine our new observational data with a typical model that has been used before. Thus we follow the basic scheme devised by Murai & Fujimoto (1980). Once we have characterized this conventional prescription, we then ask in a forthcoming paper which, if any, of the parameters need to be changed in order to better match observed features of the MC-MW system such as the Magellanic Stream.

Gravitational Potentials:
We represent the gravitational potential of the Galaxy, as a function of distance from the

center, by an isothermal halo distribution:

$$\phi_G(r) = -V_0^2 \ \ln r, \tag{5}$$

where $V_0 = 220$ km s^{-1} is the circular velocity which is assumed to be constant far outside the disk. The total mass enclosed within a sphere of radius r kpc is

$$M_G(< r) = 5.6 \times 10^{11} \left(\frac{V_0}{220 \text{ km s}^{-1}} \right)^2 \left(\frac{r}{50\text{kpc}} \right) M_\odot. \tag{6}$$

It is possible that the Galactic potential beyond the present location of the Clouds is triaxial, and in principle, the results of this study in combination with the morphology of the MS can be used to test this. However, a significant departure from spherical symmetry would induce a precession in the orbital plane of a satellite (e.g. Fellhauer et al. 2006). The lack of a noticeable warp in the Stream in either position in the sky or radial velocity space suggests that the assumption of spherical symmetry is a good one at least to first order (Lin et al. 1995), although admittedly we do not have any distance or proper motion information for the Stream. We do not employ a cut-off radius for the extent of the dark halo. This is a reasonable assumption since the halo is thought to enclose the current orbits of the Clouds.

The LMC and SMC are represented using Plummer models:

$$\phi_{L,S}(r) = GM_{L,S}/[(\mathbf{r} - \mathbf{r}_{L,S})^2 + K_{L,S}^2]^{1/2}, \tag{7}$$

with effective radii (K_L, K_S) of 3 and 2 kpc respectively.

The Masses of the Clouds:
The most serious uncertainty in the model input parameters arises from the lack of precise determinations of the masses of the Clouds. The masses of the Clouds will play a role in determining the amount of dynamical friction that they feel from the MW, and they will determine to what extent they are bound to each other. The latest observational data imply a range of possible masses. A dynamical mass for the LMC within 8.9 kpc of $(8.7 \pm 4.3) \times 10^9$ $M_\odot$ was obtained by van der Marel et al. (2002) using an analysis of carbon stars. This is less than half of the mass adopted in previous studies. For example, Gardiner & Noguchi (1996; hereafter GN96) adopted a value of 2×10^{10} $M_\odot$. This was estimated by Schommer et al. (1992) from radial velocities of several of the oldest star clusters in the LMC that lie well beyond 6 kpc of its center.

Our own measurements give a relative velocity between the Clouds at the current epoch of 105 ± 42 km s^{-1} . For comparison, we can calculate the escape velocity of the SMC from the LMC, $v_{e,\text{SMC}}$, assuming a simple point mass geometry. Using the value of 2×10^{10} $M_\odot$ for the mass of the LMC and 23 kpc for the distance between the Clouds, we get

$v_{e,\rm SMC} = \sqrt{2GM_L/r} = 87$ km s^{-1} . This is consistent with the observed relative velocity at 1σ confidence. But the LMC would need to have mass $M_L = 3 \times 10^{10} M_\odot$ if the Clouds are gravitationally bound and the relative velocity is as large as 105 km s^{-1} . Given the range of possible masses, we do not systematically search the parameter space of LMC mass in our models, but rather consider three cases for $M_L = 1, 2$ & 3×10^{10} $M_\odot$.

For the SMC, a lower mass limit of 1×10^9 $M_\odot$ was obtained by Hardy et al. (1989) from observations of carbon stars and Dopita et al. (1985) from planetary nebulae. Both of these measurements were made close to the SMC center, so its mass is probably much larger. More recently, Zartisky & Harris (2006) used a virial analysis of the kinematics of 2046 red giant stars in the SMC to obtain an enclosed mass within 1.6 kpc of between 1.4 and $1.9 \times 10^9 M_\odot$ and a mass within 3 kpc of between 2.7 and $5.1 \times 10^9 M_\odot$. This has prompted us to take a typical value for the mass of the SMC of $M_S = 3 \times 10^9$ $M_\odot$.

We do not include any effects of mass-loss in the fiducial model. Mass-loss is probably significant given the amount of matter in the MS (estimated to be $\sim 2 \times 10^8$ $M_\odot$ according to Putman et al. (2003)). This is obviously an oversimplification, but should still serve as a basic picture of the overall dynamics of the Clouds, given that we are not attempting to model the Magellanic Stream.

Dynamical friction:
The effect of dynamical friction on the orbits of the Clouds as they pass through the dark halo of the Galaxy is taken into account as in previous studies using the expression from Binney & Tremaine (1987):

$$\mathrm{F}_G = -0.428 \ln \Lambda_G \, \frac{G M_{L,S}^2}{r^2}. \tag{8}$$

Here r is the distance between each Cloud and the center of the Galaxy. The Coulomb logarithm $\ln \Lambda_G$ of both Clouds is taken as 3.0 (Binney & Tremaine 1987). This assumes as a simplification that the orbits are circular. Equation (7) is generally a good approximation to the full expression for dynamical friction

$$\frac{d\mathbf{v}}{dt} = -\frac{4\pi \ln \Lambda G^2 \rho M}{v^3} \left\{ [\mathrm{erf}(X) - \frac{2X}{\sqrt{\pi}} e^{-X^2}] \mathbf{v} \right\}_{X = v/V_0}, \tag{9}$$

which does not make the assumption of circular orbits explicitly. Our experience shows that small differences only start to build up between the two terms if the orbits are integrated quite far backward in time (on the order of ~ 10 Gyr).

We also take into account the dynamical friction between the LMC and the SMC, following Bekki & Chiba (2005):

$$\mathrm{F}_{LS} = -0.428 \ln \Lambda_{LS} \frac{G M_S^2}{r_{LS}^2}, \tag{10}$$

where $\ln \Lambda_{LS} = 0.2$ and r_{LS} is the distance between the two Clouds. This force is assumed to act on the SMC when it comes within the tidal radius of the LMC, which in this study is adopted as 15 kpc (van der Marel et al. 2002). The associated gain in angular momentum to the orbit of the LMC is found to be negligible in our models. This makes sense given the mass ratio between the two Clouds $(3-10)$. Any energy gain felt by the LMC is not expected to affect its orbital motion but would instead go into puffing up its halo (e.g. Weinberg 2000). Thus we do not include any additional force terms for the LMC.

As we will discuss in § 6.2, one of the striking results of our models for the orbits of the Clouds is that it is very difficult to keep them bound to each other for more than 1 Gyr in the past. Dynamical friction between the Clouds, if significant, would make this situation worse, since it would act to coalesce the orbit of the SMC with that of the LMC and thus imply that they were on even more disparate trajectories in the past. Thus for our fiducial model we also investigate orbits in which we do not include dynamical friction between the Clouds. This is justified as a first-order solution because 1) the distribution of dark matter in the LMC is not very well known, and 2) if dynamical friction was a significant factor, and the Clouds have been a bound system for approximately a Hubble time, then they probably would have merged already.

5.2. The Search for Bound Orbits

We propagate the orbits of both Clouds backward in time for 9 Gyr using the fiducial model described above and a leapfrog integration scheme outlined in Springel et al. (2001). The equations of motions for the Clouds about a stationary Galaxy can be written down using the equations in § 5.1:

$$\frac{d^2\mathbf{r}_L}{dt^2} = \frac{\partial}{\partial \mathbf{r}_L}[\phi_S(\mid \mathbf{r}_L - \mathbf{r}_S \mid) + \phi_G(\mid \mathbf{r}_L \mid)] + \frac{\mathrm{F}_L}{M_L}\frac{\mathbf{v}}{v} \tag{11}$$

and

$$\frac{d^2\mathbf{r}_S}{dt^2} = \frac{\partial}{\partial \mathbf{r}_S}[\phi_L(\mid \mathbf{r}_S - \mathbf{r}_L \mid) + \phi_G(\mid \mathbf{r}_S \mid)] + \frac{\mathrm{F}_S}{M_S}\frac{\mathbf{v}}{v}. \tag{12}$$

For our mean estimates of proper motion (quoted in equation (3) in Paper I and equation (1) in this paper), and ignoring the error bars, we find that the Clouds become unbound from each other very quickly in the past. It is therefore interesting to see if *any* orbits in our proper motion error ellipses will remain bound for a significant fraction of a Hubble time.

We used a simple Monte Carlo scheme to draw twelve initial phase-space coordinates from the errors subtended by the parameters in Table 3. From these initial phase-space coordinates we then calculated the initial values of position and velocity for both Clouds in

a Galactocentric reference system. We then propagated the orbits of both Clouds backward in time for 9 Gyrs using the fiducial model described above. This procedure was repeated 10,000 times. For each orbit we kept track of when the Clouds moved more than 50 kpc from each other and labeled this time as the "time of disruption" of the bound system (following GN96). Further, we repeated this exercise for a few cases of Cloud mass, each with the inclusion of dynamical friction between the Clouds and without.

For each orbit in a given Monte Carlo run, we kept track of the initial proper motions (at time zero, i.e. the present time) and color-coded them according to outcome : red if the Clouds stayed together for more than 5 Gyr ("bound orbits"), green if they stayed together for between 1 and 5 Gyrs, and black if they disrupted within a Gyr. Figures 11 and 12 are representative of the results of the exercise as a whole but show the specific case of $M_L = 3 \times 10^{10}\ M_\odot$ and $M_S = 3 \times 10^9\ M_\odot$ without the inclusion of dynamical friction between the Clouds. Figure 11 shows the results in proper motion space and Figure 12 shows the results in velocity space. Given our fiducial model, one can draw from a significant fraction of the LMC error ellipse, although the southwest portion is more favorable, and get orbits that have been bound for a significant portion of the past Hubble time. For the SMC, bound orbits are much more probable if we draw from the southeast portion of its error ellipse. The locations of the mean values of the bound regions are not overly dependent on the input masses of the Clouds, or the inclusion of dynamical friction between the Clouds. In general, however, a more massive LMC requires less of a shift in the proper motions of both Clouds to bind the SMC, as expected. Thus we do find bound orbits within our proper motion error ellipses.

Figure 13 is a representative bound orbit that we chose at random from the simulation. The Galactocentric distance of the LMC is shown in black, that of the SMC is shown in red and the Galactocentric distance of the center of mass of the two Clouds is shown in green (this is indistinguishable from the LMC's motion). The distance between the Clouds is shown in blue. The center of mass has an orbital period of ~ 2.5 Gyr and an inclination of 103° (with respect to the plane of the Galactic disk).

The number of bound orbits does depend on the masses of the Clouds and whether dynamical friction between the Clouds is included. However, this difference is not very significant. While the bound fraction increases with increasing LMC mass, it is very small in all cases. The bound fraction ranges from 3% for LMC mass $= 1 \times 10^{10} M_\odot$ to 10% for LMC mass $= 3 \times 10^{10} M_\odot$ for models without dynamical friction between the Clouds included. It remains roughly at 2% for models with dynamical friction between the Clouds. We discuss the implications of our Monte Carlo simulations in the next section. The fraction of bound orbits always increases when the LMC or SMC masses are increased. On the basis of the

presently available kinematic data for these galaxies it cannot be ruled out that they have massive dark halos that extend for tens of kpcs. Such halos would make the galaxies more massive than has been assumed here, and would increase the fraction of orbits consistent with our proper motion data that are bound.

5.3. Interpretation of Orbit Calculations

The percentages of bound orbits in our Monte Carlo simulations (quoted above) should not be interpreted as probability estimates for whether the Clouds are bound or not. The small number of bound orbits is more likely due to the large observational error bars and the comparatively small phase-space spanned by bound orbits in a three-body problem. Our results are consistent with the outcome of most past searches for bound orbits for the Clouds (see e.g. Appendix A of Bekki & Chiba 2005, or Fig. 2 of Gardiner et al. 1994) in which authors have found that a very small fraction of orbits searched in this fiducial model will remain bound. Our SMC error bars are not small enough to either confirm or rule out that the Clouds have been a bound system. Given the results of our simulations, however, it is worthwhile to further investigate whether there are indications that some unidentified systematic error might be present in the data.

The proper motion of the LMC and the associated uncertainty should be solid. As demonstrated in Paper I we had 21 QSO fields all taken at different roll angles of the telescope, thus allowing any systematic errors tied to the CCD frame to average out roughly as $1/\sqrt{N}$. We did a number of consistency checks that showed no indication of systematic effects. In the case of the SMC, however, we have far fewer fields, and 3 out of the 4 reliable QSO fields were taken with the same orientation of the camera. So if there were systematic errors tied to the CCD frame (e.g. due to inaccuracies in the ACS HRC geometric distortion correction) then they would not have averaged out as they did for the LMC. As a final consistency check on our data, we have thus sought to answer the following question : if we keep the LMC proper motion fixed at our best estimate values, what values of SMC proper motion give rise to bound orbits? To answer this we kept the model fixed at the fiducial model (with $M_L = 2 \times 10^{10} M_\odot,\ M_S = 3 \times 10^9 M_\odot$), searched a grid in SMC proper motion space from -2 to 2 mas yr^{-1} in the north-south and east-west directions, and then looked for initial SMC proper motion values that gave rise to bound orbits (for > 5 Gyr).

Figure 14 shows the results. It is a plot of the grid in SMC proper motion space that was searched with the duration of the bound state represented by points of different colors: black for < 1 Gyr, green for between 1 & 5 Gyr and red for > 5 Gyr. Figure 15 is the same but shows the results in velocity space. The red region in Figure 14 has a mean value

of $\mu_W = -1.35 \pm 0.12$ mas yr^{-1} , $\mu_N = -1.45 \pm 0.13$ mas yr^{-1} , which is an approximate 1σ shift from our measured value of SMC proper motion in the westward direction, and $\sim 1.5\sigma$ in the northward direction. These values are stated for reference only because the red region should not be interpreted as a Gaussian error region. Every orbit in this region is acceptable, and the only requirement is that the 1σ errors of our data (shown with a black ellipse) have non-zero overlap with the red region. This seems to be the case. What this means is that, given the error bars, our measurement for the SMC proper motion falls where it is expected to be based on the LMC proper motion and the assumption that the Clouds are a bound system. Conversely, if both our LMC and SMC proper motion measurements had some unidentified systematic error then this would most likely have yielded orbits that are unbound. The fact that bound orbits exist within the error regions of our data is therefore a strong argument that our measurements and error estimates are realistic.

5.4. The 'Recent Coupling' Model

Our SMC proper motion is consistent with a bound status for the Clouds. But, while we do find bound orbits in our Monte Carlo simulations, we also find many disrupted ones. It thus remains possible that the Clouds are not a bound system and have only interacted long enough to produce the Stream. Most models of the Stream suggest that this happened during their last perigalactic passage. There is some evidence in the literature for the Clouds having become dynamically coupled only recently.

Bekki & Chiba (2005) find that in their models, even with such small total and relative velocities between the Clouds as those that have gone into the theoretical modeling thus far (GN96), it is very hard for the Clouds to maintain their bound status for very long backward in time. They discuss a recent coupling scenario for the formation of the Clouds, and argue that this has the following advantages. First, it takes into account dynamical friction between the Clouds. Second, the LMC has an asymmetric and irregular distribution of young clusters and star-formation regions (van den Bergh 2000) and a scenario that has the LMC uncoupled from the SMC might shed some light on their formation history. Specifically, it might explain the 'age gap' problem in the LMC, i.e. the presence of only one Globular Cluster (GC) which was formed between 13 & 3 Gyr ago. Such a gap is not seen in the SMC (Piatti et al. 2002, Da Costa 1991). Since it is thought that strong tidal perturbations trigger the formation of clusters (e.g. Whitmore 1999), it is not clear why they would not have been continuously produced in the LMC, since if the Clouds are a bound system they would have been tidally perturbing each other for the past 15 Gyr. Bekki & Chiba argue that this can be understood in terms of the recent coupling model as follows: the LMC was

formed as a low surface brightness galaxy far enough from the Galaxy (they estimate 150 kpc from the old data) that the Galactic tidal field could not trigger cluster formation till the LMC first encountered the SMC. The SMC was formed closer and being less massive was more influenced by the Galactic tide and formed GCs continuously. So to sum up, the difference in cluster formation histories between the Clouds can perhaps be explained by the differences in birth locations and initial masses of the Clouds.

Despite the arguments of Bekki & Chiba (2005), a model in which the Clouds have always been a bound system is very compelling. The common HI envelope that surrounds the Clouds indicates that they have been associated with each other at least for some time. Given the sparse distribution of outer satellites of the Galaxy, a capture event of the SMC by the LMC seems improbable (GN96). The bound models pursued in previous theoretical works have been able to reproduce the structure and kinematics of the Magellanic Stream. Such models have also been used to explain star formation about 0.2 Gyr ago in the LMC disk (Gardiner et al. 1994), the structure of the stellar halo, and the recent star formation history of the SMC (GN96; Yoshizawa & Noguchi 2003). However, as Bekki & Chiba (2005) point out, it is not clear whether models that do not make the explicit assumption of bound orbits could explain all these features equally well.

6. Summary & Future Work

We obtained two epochs of ACS HRC data to determine the proper motions of the LMC & SMC with respect to a sample of background QSOs distributed homogeneously behind the central few degrees of both galaxies. Our result for the SMC is presented here. With 4 QSOs and an approximately 2 year-long baseline, we have determined the proper motion of the SMC to be $\mu_W = -1.16 \pm 0.18$ mas yr^{-1}, $\mu_N = -1.17 \pm 0.18$ mas yr^{-1} . This is the best available measurement of its proper motion and is accurate to 15%. We have carried out a suite of tests to robustly quantify both random and systematic errors. We use our LMC (from Paper I) and SMC proper motion estimates to investigate the past orbital evolution of both Clouds around the Milky Way. We find that while our data are consistent with orbits in which the Clouds have been bound to each other for approximately a Hubble time, there are also many unbound orbits within the error circles. So even though our errors on the SMC's motion are the most accurate thus far, they are not sufficient to uniquely say whether the Clouds are indeed bound. Also, it should be noted that our treatment of the orbits as a restricted few-body interaction within a fixed Milky Way potential is oversimplified. Structure formation in the Universe proceeds hierarchically and it is unrealistic to assume that the mass and properties of the galaxies involved were the same many Gyrs ago as they

are now. For example, over the past 9 Gyr the mass of the Galaxy has probably increased by a factor of two (e.g. Bullock & Johnston 2005). Full cosmological simulations will be required to take this into account properly.

Now that the space velocities of both Clouds are well-characterized, it will be worthwhile to combine this information with the morphology and radial velocity of the Magellanic Stream to place constraints on the potential of the Galactic halo. The natural next step in this project is therefore to vary the prescription of the Galaxy model and quantify what type of halo would best match the Stream, given the observed LMC & SMC three-dimensional velocities. This will be the subject of a forthcoming paper. The parameters that this should constrain are the axial ratio of the halo, the slope of the circular velocity curve beyond ~ 50 kpc, and the implied Galactic mass at that distance. There are few other kinematic tracers at this location that can be used for such a measurement. Thus the combination of the orbital information of the Clouds and the morphology of the Magellanic Stream will provide a valuable new constraint. Combination of the orbital information of the MCs and the Magellanic Stream with tidal streams from other Local Group dwarfs such as the Sagittarius Stream (Ibata et al. 1994; Majewski et al. 2003) might further constrain the potential of the halo (e.g. Fellhauer et al. 2006; Belokurov et al. 2006; Johnston et al. 2005; Law et al. 2005; Helmi 2004).

The present-day velocities of the clouds assumed in models of the Stream have spanned a considerable range. However, most authors who have investigated tidal models for the origin of the Stream have used the assumed present-day velocities suggested by GN96. These differ from our observed values (given in Table 3) by 109 ± 16 km s^{-1} for the LMC and 142 ± 50 km s^{-1} for SMC (where each listed value is the length of the three-dimensional residual vector). So our measurements are not consistent with these models. Therefore, even without detailed calculations it is clear that revisions may be necessary to bring existing models into accordance with our observations. Previous models for the Stream have generally assumed a spherical logarithmic potential for the dark halo. It might be necessary to deviate from this simple prescription to obtain a good fit to the Stream given the observed present-day velocities. As mentioned, this would provide new insight into the properties of the Milky Way dark halo. But there are many other uncertainties in existing models as well. Probably the biggest uncertainties reside in the total mass and mass profiles of the Clouds themselves. Future models may also need to incorporate more details of the processes of hydrodynamics, mass loss, and star formation. Conversely, tighter constraints on the dynamical evolution of the Clouds may provide a better picture of the star formation histories of the Clouds.

An important outcome of this work is the evidence that *HST* is stable enough to provide good proper motions using relatively short baselines. However, future improvements to our

estimate of the SMC's proper motion should be possible by using a longer baseline and a larger sample of QSOs. In addition to the Geha et al. (2003) MACHO sample, QSOs behind the SMC have also been found from the OGLE database (Dobrzycki et al. 2003). Even though the mass distribution of the MCs remain the largest source of uncertainty, smaller errors on the SMC's motion would greatly reduce the observational phase space. This may allow us to definitively say whether the Clouds are bound to each other. Hence, an additional epoch of data would be valuable. With astrometric missions such as SIM and $GAIA$ a rather long time down the road, HST can continue to make important contributions to these subjects for several years to come.

The authors would like to thank Jay Anderson for making his geometric distortion calibration software available to us. NK would like to thank Brant Robertson, Gurtina Besla, Lars Hernquist and Matthew Holman for very useful discussions about orbits. NK is also grateful to Dana Dinescu for pointing out some SMC proper motion work in the literature, and to Pavlos Protopapas for useful discussions about the project as a whole. Support for this work was provided by NASA through grant numbers associated with projects GO-09462 and GO-10130 from the Space Telescope Science Institute (STScI), which is operated by the Association of Universities for Research in Astronomy, Inc., under NASA contract NAS5-26555.

7. References

Anderson, J. & King, I. R. 2004a, ACS Instrument Science Report 04-15 (Baltimore: Space Telescope Science Institute)
Anderson, J., & King, I. R. 2004b, AJ, 128, 950
Belokurov, V., et al. 2006, ApJ, 642, L137
Bekki, K., & Chiba, M. 2005, MNRAS, 356, 680
Binney, J. & Tremaine, S. 1987, Galactic Dynamics, (Princeton: Princeton Univ. Press)
Bullock, J. S., & Johnston, K. V. 2005, ApJ, 635, 931
Caldwell, J. A. R., & Coulson, I. M. 1986, MNRAS, 218, 223
Cioni, M.-R. L., van der Marel, R. P., Loup, C., & Habing, H. J. 2000, A&A, 359, 601
Connors, T. W., Kawata D., Gibson B. K. 2005 astro-ph/0508390
Cole, A. A., Tolstoy, E., Gallagher, J. S., & Smecker-Hane, T. A. 2005, AJ, 129, 1465
Crowl, H. H., Sarajedini, A., Piatti, A. E., Geisler, D., Bica, E., Clariá, J. J., & Santos, J. F. C. 2001, AJ, 122, 220
Da Costa, G. S. 1991, IAU Symp. 148: The Magellanic Clouds, 148, 183
Dobrzycki, A., Macri, L. M., Stanek, K. Z., & Groot, P. J. 2003, AJ, 125, 1330

Dolphin, A. E., Walker, A. R., Hodge, P. W., Mateo, M., Olszewski, E. W., Schommer, R. A., & Suntzeff, N. B. 2001, ApJ, 562, 303
Dopita, M. A., Lawrence, C. J., Ford, H. C., & Webster, B. L. 1985, ApJ, 296, 390
Fellhauer, M. et al. 2006 astro-ph/0605026
Font, A. S., Johnston, K. V., Bullock, J. S., & Robertson, B. E. 2006, ApJ, 638, 585
Freedman, W. L., et al. 2001, ApJ, 553, 47
Freire, P. C., Camilo, F., Kramer, M., Lorimer, D. R., Lyne, A. G., Manchester, R. N., & D'Amico, N. 2003, MNRAS, 340, 1359
Gardiner, L. T., & Noguchi, M. 1996, MNRAS, 278, 191 (GN96)
Gardiner, L. T., Sawa, T., & Fujimoto, M. 1994, MNRAS, 266, 567
Geha, M. et al. 2003, AJ, 125, 1
Haberl, F., Filipović, M. D., Pietsch, W., & Kahabka, P. 2000, A&AS, 142, 41
Hardy, E., Suntzeff, N. B., & Azzopardi, M. 1989, ApJ, 344, 210
Harris, J., & Zaritsky, D. 2006, AJ, 131, 2514
Harris, J., & Zaritsky, D. 2001, ApJS, 136, 25
Hatzidimitriou, D., Cannon, R. D., & Hawkins, M. R. S. 1993, MNRAS, 261, 873
Heller, P. & Rohlfs, K. 1994, A&A, 291, 743
Helmi, A. 2004, ApJ, 610, L97
Hernquist, L. 1990, ApJ, 356, 359
Holtzman, J. A., et al. 1997, AJ, 113, 656
Ibata, R. A., Gilmore, G., & Irwin, M. J. 1994, Nature, 370, 194
Irwin, M. 1999, IAU Symposium, 192, 409
Irwin, M., Demers, S., & Kunkel, W. 1996, Bulletin of the American Astronomical Society, 28, 932
Johnston, K. V., Law, D. R., & Majewski, S. R. 2005, ApJ, 619, 800
Johnston, K. V., Zhao, H., Spergel, D. N., & Hernquist, L. 1999, ApJ, 512, L109
Kallivayalil, N., van der Marel, R. P., Alcock, C., Axelrod, T., Cook, K. H., Drake, A. J., & Geha, M. 2006, ApJ, 638, 772
Krist, J. 2003, ACS Instrument Science Report 03-06 (Baltimore: Space Telescope Science Institute)
Kroupa, P. & Bastian, U. 1997, New Astronomy, 2, 77
Law, D. R., Johnston, K. V., & Majewski, S. R. 2005, ApJ, 619, 807
Lin, D. N. C., & Lynden-Bell, D. 1982, MNRAS, 198, 707
Lin, D. N. C., Jones, B. F., & Klemola, A. R. 1995, ApJ, 439, 652
Majewski, S. R., Skrutskie, M. F., Weinberg, M. D., & Ostheimer, J. C. 2003, ApJ, 599, 1082
Mastropietro, C., Moore, B., Mayer, L., Wadsley, J., & Stadel, J. 2005, MNRAS, 363, 509
Mathewson, D. S., Ford, V. L., & Visvanathan, N. 1986, ApJ, 301, 664

Mathewson, D. S., Cleary, M. N., & Murray, J. D. 1974, ApJ, 190, 291
Momany, Y., & Zaggia, S. 2005, A&A, 437, 339
Moore, B., & Davis, M. 1994, MNRAS, 270, 209
Muñoz et al. 2006 astro-ph/0605098
Murai, T., & Fujimoto, M. 1980, PASJ, 32, 581
Navarro, J. F., Frenk, C. S., & White, S. D. M. 1997, ApJ, 490, 493
Peñarrubia, J., et al. 2005, astro-ph/0512507
Piatti, A. E., Sarajedini, A., Geisler, D., Bica, E., & Clariá, J. J. 2002, MNRAS, 329, 556
Putman, M. E., et al. 1998, Nature, 394, 752
Putman, M. E., Staveley-Smith, L., Freeman, K. C., Gibson, B. K., & Barnes, D. G. 2003, ApJ, 586, 170
Schommer, R. A., Suntzeff, N. B., Olszewski, E. W., & Harris, H. C. 1992, AJ, 103, 447
Smecker-Hane, T. A., Cole, A. A., Gallagher, J. S., III, & Stetson, P. B. 2002, ApJ, 566, 239
Springel, V., Yoshida, N., & White, S. D. M. 2001, New Astronomy, 6, 79
Stanimirović, S., Staveley-Smith, L., & Jones, P. A. 2004, ApJ, 604, 176
van den Bergh, S. 2000, The galaxies of the Local Group, Cambridge, UK: Cambridge University Press
van der Marel, R. P., Alves, D. R., Hardy, E., & Suntzeff, N. B. 2002, AJ, 124, 2639
Wannier, P., & Wrixon, G. T. 1972, ApJ, 173, L119
Wayte, S. R. 1991, IAU Symp. 148: The Magellanic Clouds, 148, 447
Welch, D. L., McLaren, R. A., Madore, B. F., & McAlary, C. W. 1987, ApJ, 321, 162
Weinberg, M. D., & Blitz, L. 2006, ApJ, 641, L33
Weinberg, M. D. 2000, ApJ, 532, 922
Westerlund, B. E. 1997, The Magellanic Clouds (Cambridge: Cambridge Univ. Press)
Whitmore, B. C. 1999, IAU Symp. 186: Galaxy Interactions at Low and High Redshift, 186, 251
Yoshizawa, A. M., & Noguchi, M. 2003, MNRAS, 339, 1135
Zentner, A. R., & Bullock, J. S. 2003, ApJ, 598, 49

Table 1. Sample and Observations

ID	QSOname	RA	DEC	V	z	epoch1					epoch2				Δtime
						date	visit	T_{exp} F606W	T_{exp} F814W	ORIENTAT	date	visit	T_{exp} F606W	ORIENTAT	
		(H,M,S)	(deg, ', ")					(min)	(min)	(deg)			(min)	(deg)	(yrs)
S1	208.16034.100	00 51 17.0	-72 16 51.3	18.6	0.49	2002-08-27	14	6.7	1.7	140.8	2004-07-16	13	9.5	95.9	1.9
S2	207.16316.446	00 55 34.7	-72 28 33.9	18.9	0.56	2002-08-26	15	6.7	1.7	137.4	2004-07-17	14	9.6	96.1	1.9
S3	211.16703.311	01 02 14.5	-73 16 26.6	20.3	2.18	2002-09-03	16	6.7	1.7	129.6	2004-07-13	15	16	90.8	1.9
S4	QJ0036-7227	00 36 39.7	-72 27 42.0	19.6	1.62	2002-09-13	17	8	1.7	160.9	2005-06-19	16	18	72.1	2.8
S5	211.16765.212	01 02 34.7	-72 54 23.8	18.4	2.13	2003-02-15	36	6.7	1.7	-51.1	2004-07-15	33	6.7	91.5	1.4

Note. — Column 1 is a field identification. Column 2 gives the MACHO ID for referencing with Geha et al. (2003). Columns 3 & 4 give the RA and Dec of the QSOs (J2000). The V magnitudes quoted in column 5 are from our HST data. Column 6 gives the QSO redshifts. S4 is a ROSAT object from Haberl et al. (2000). All other redshifts are from Geha et al. (2003). Epoch 1 has program ID 9046 (Cycle 11) and epoch 2 has program ID 10130 (Cycle 13). The date of observation, HST phase II visit number, and exposure time for each field are listed. ORIENTAT is the position angle on the sky of the detector y-axis (in degrees east of north), and Δtime gives the baseline.

Table 2. Results

ID	$N_{\rm sources}$	$N_{\rm master}$	$N_{\rm used}$[a]	μ_N	μ_W	$\delta\mu_N$	$\delta\mu_W$	Used?
				(mas yr^{-1})	(mas yr^{-1})	(mas yr^{-1})	(mas yr^{-1})	
S1	247	71	32	-1.136	-0.860	0.095	0.113	Yes
S2	303	117	54	-1.208	-0.825	0.076	0.073	Yes
S3	235	87	45	-1.201	-1.022	0.109	0.091	Yes
S4	68	10	4	-0.866	-0.303	0.177	0.073	No
S5	242	100	42	-1.143	-1.471	0.130	0.108	Yes

[a] $N_{\rm sources}$ refers to the number of real sources (detected in at least half of the images). $N_{\rm master}$ refers to the number or sources in the master-list, i.e. detected in every image in every epoch. $N_{\rm used}$ refers to the number of sources that are used in the final linear transformations after the PM and δPM cuts. Columns 5-8 contain the PM estimates and their errors for each field. The last column notes if the particular field was used in our final estimate of the center of mass motion of the SMC (Equation (1)).

Table 3. Orbital Parameters

	LMC	SMC	References
Line-of-sight velocity (km s^{-1})	262.1 ± 3.4	146 ± 0.6	van der Marel et al. 2002; Harris & Zaritsky 2006
Proper Motions (W,N) (mas yr^{-1})	-2.03 ± 0.08, 0.44 ± 0.05	-1.16 ± 0.18, -1.17 ± 0.18	Paper I; this work
Distance Moduli	18.50 ± 0.1	18.95 ± 0.1	Freedman et al. 2001; Cioni et al. 2000
Current positions (α, δ) (deg)	81.9 ± 0.3, -69.9 ± 0.3	13.2 ± 0.3,-72.5 ± 0.3	van der Marel et al. 2002; Westerlund 1997; Stanimirović et al. 2004
Galactic Coordinates (l, b)	280.5, -32.5	302.8, -44.6	–
Current positions (X, Y, Z) (kpc)	$-0.8, -41.5, -26.9$	$15.3, -36.9, -43.3$	–
Space velocities (v_X, v_Y, v_Z) (km s^{-1})	$-86 \pm 12, -268 \pm 11, 252 \pm 16$,	$-87 \pm 48, -247 \pm 42, 149 \pm 37$	–
Galactocentric radial velocities (km s^{-1})	89 ± 4	23 ± 7	–
Galactocentric tangential velocities (km s^{-1})	367 ± 18	301 ± 52	–

Note. — Positions and velocities of the Clouds as discussed in the text and Paper I. The last column lists the sources of the adopted values. No source is listed for the values in the bottom 5 lines because they follow uniquely from the top 4 lines.

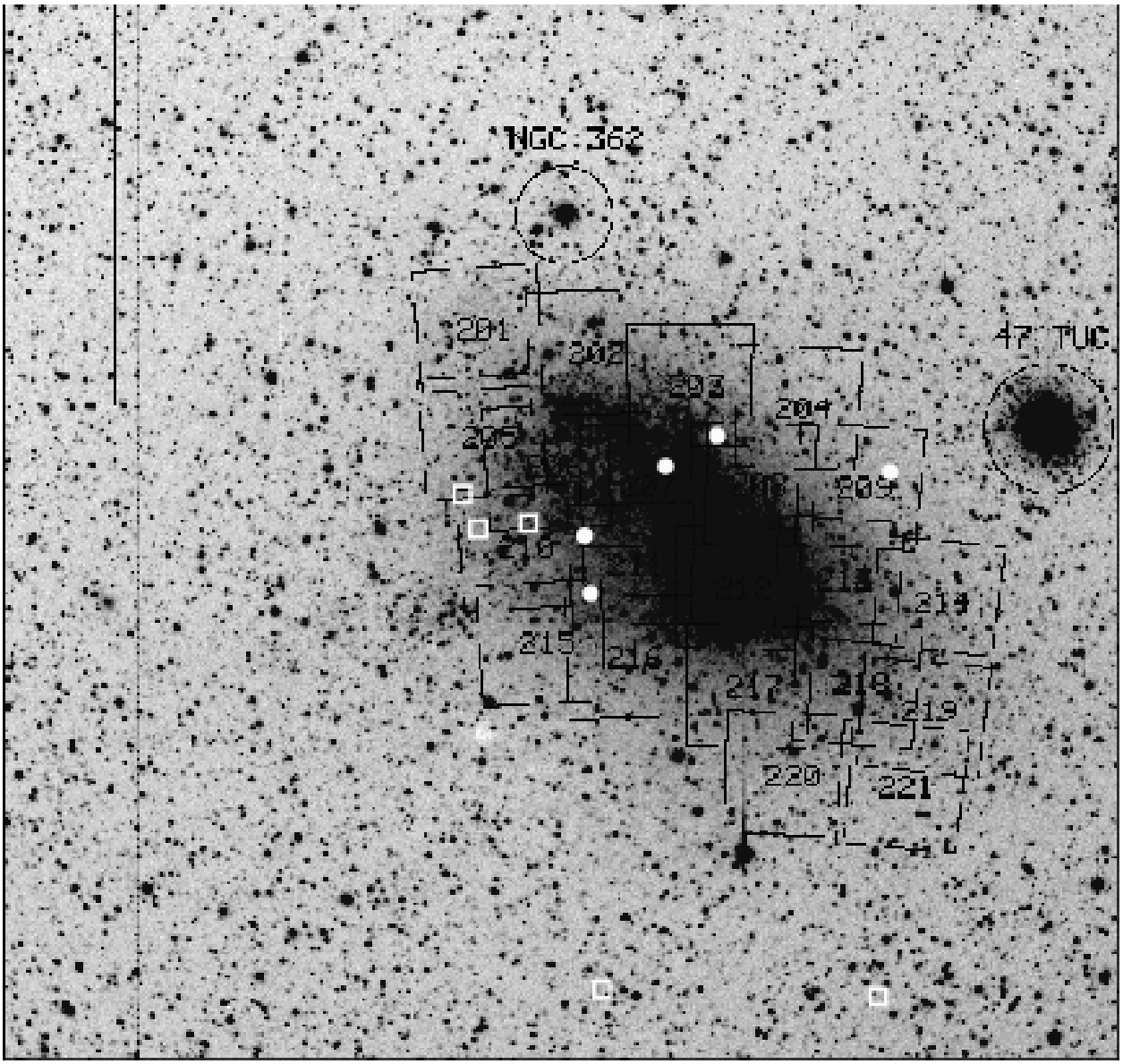

Fig. 1.— R-band image of the SMC ($4° \times 4°$). The MACHO photometric coverage is indicated (black boxes). White circles indicate reference QSOs for which we obtained two epochs of ACS/HRC imaging, squares indicate QSOs which we did propose for but for which we did not get two epochs of imaging in our snapshot program.

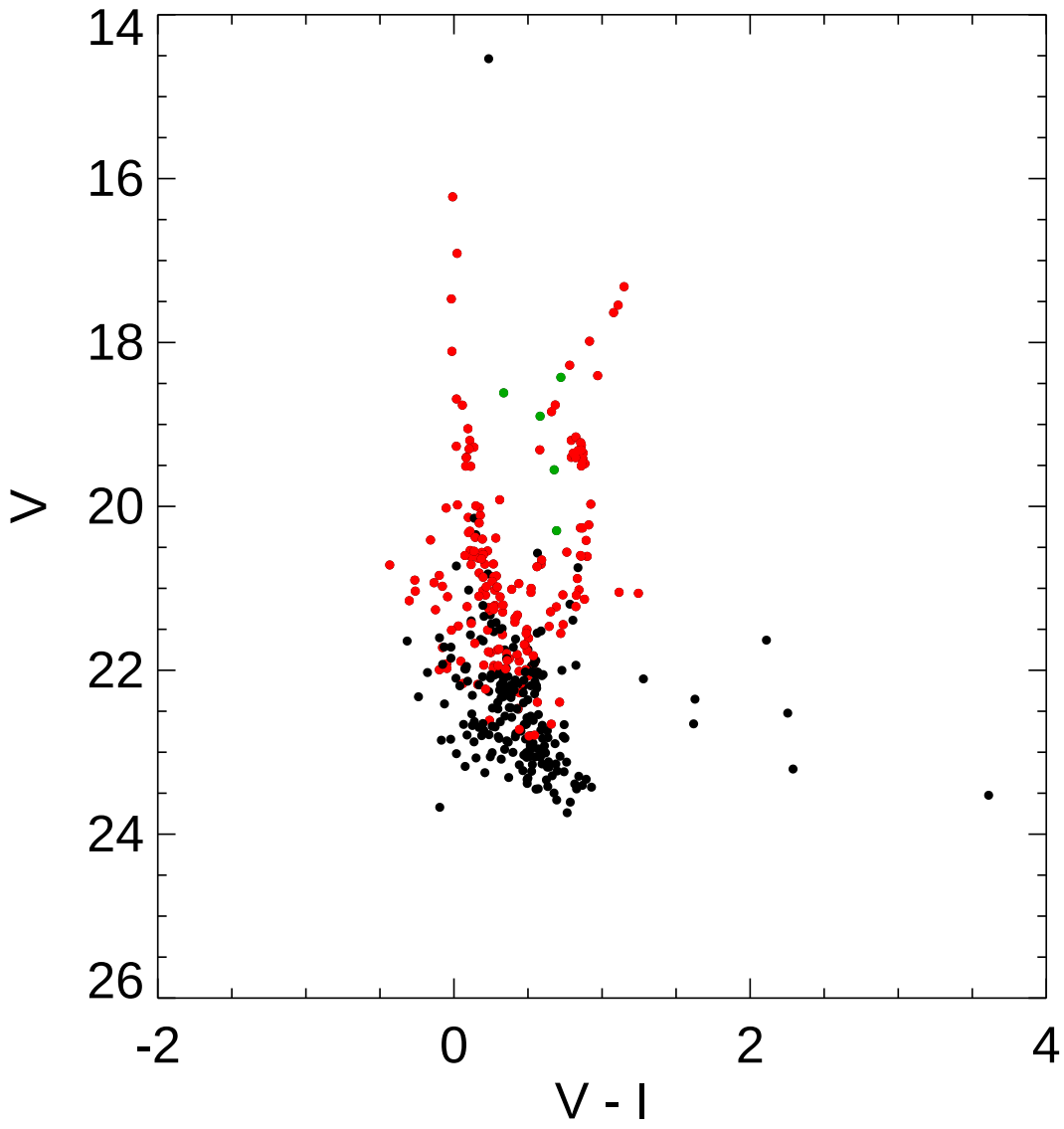

Fig. 2.— $(V-I, V)$ color-magnitude diagram for the SMC. QSOs are marked in green, stars in the master-list with PM & δPM < 0.1 pixels are marked in red and the rest are shown in black.

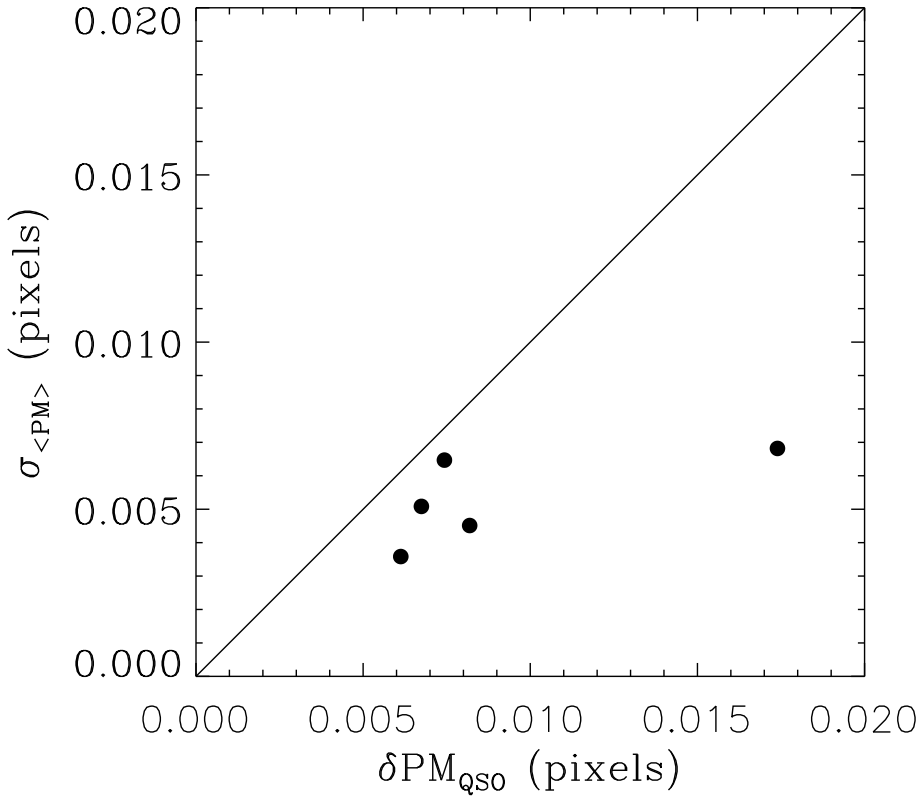

Fig. 3.— The distribution of errors in our linear transformations for each field. The x-axis shows the error in the PM of the QSO and the y-axis shows the error in the average PM of the star-field.

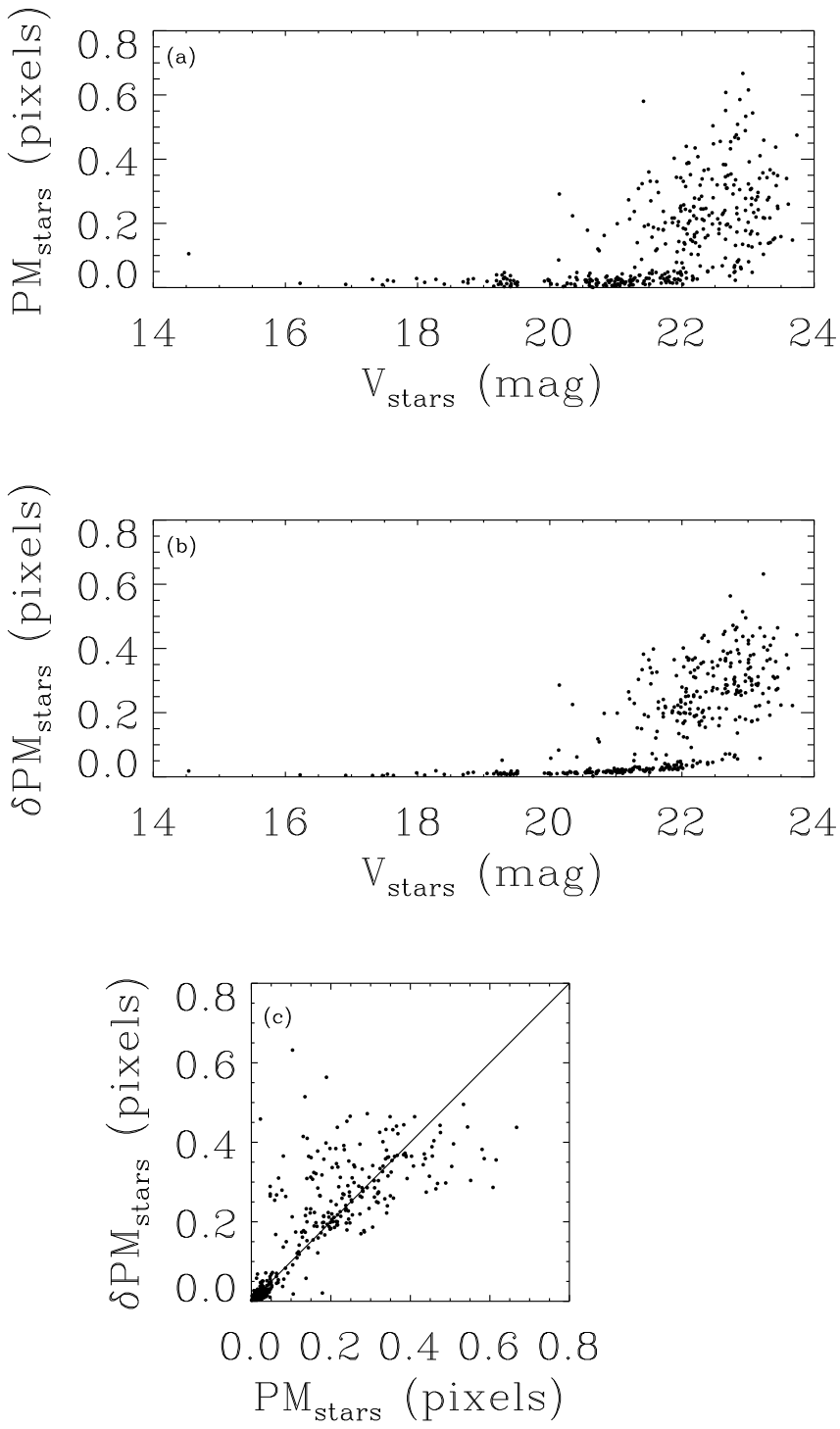

Fig. 4.— (a) PMs for all stars in all master-lists as a function of their V magnitude; (b) δPM for all stars in all master-lists as a function of V magnitude; (c) δPM vs. PM for all stars in all master-lists.

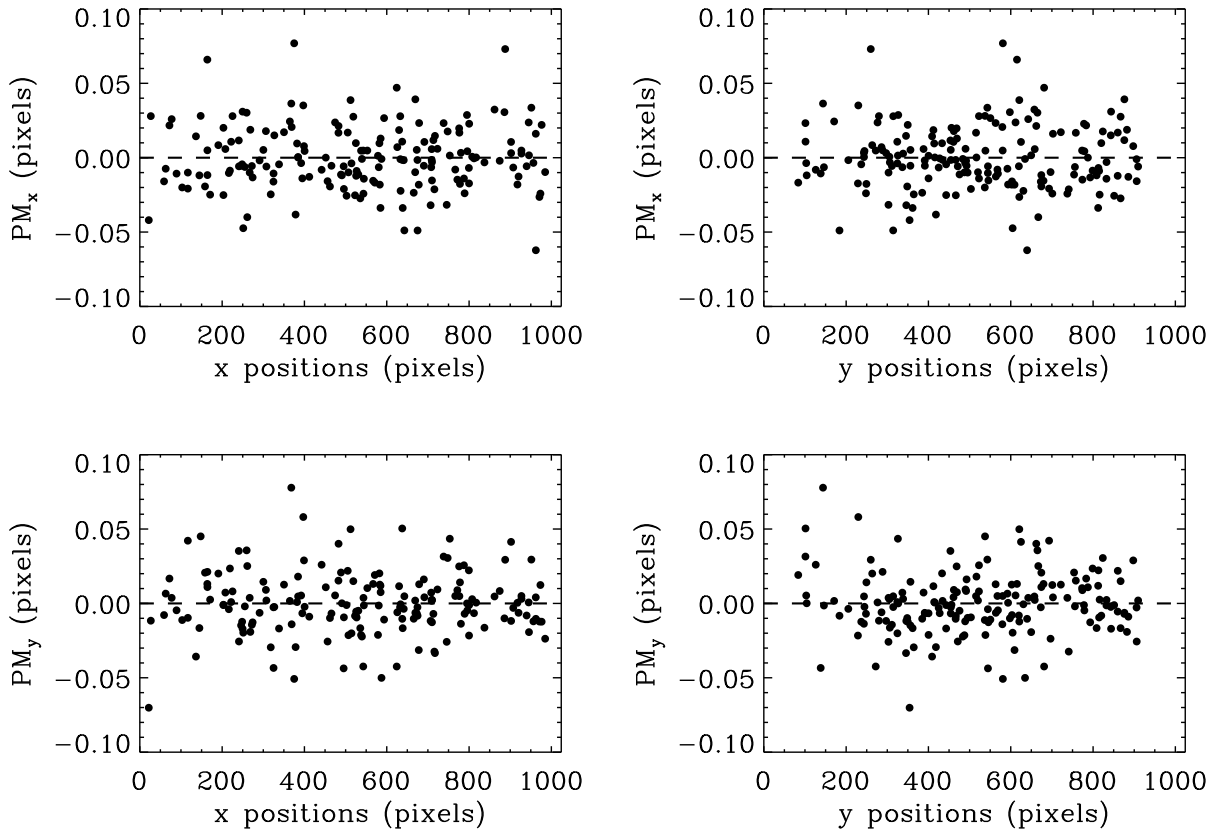

Fig. 5.— PMs of the stars in the masterlist that have PM and δPM < 0.1 pixels versus chip location separately for x and y to see if there are any systematic trends with position.

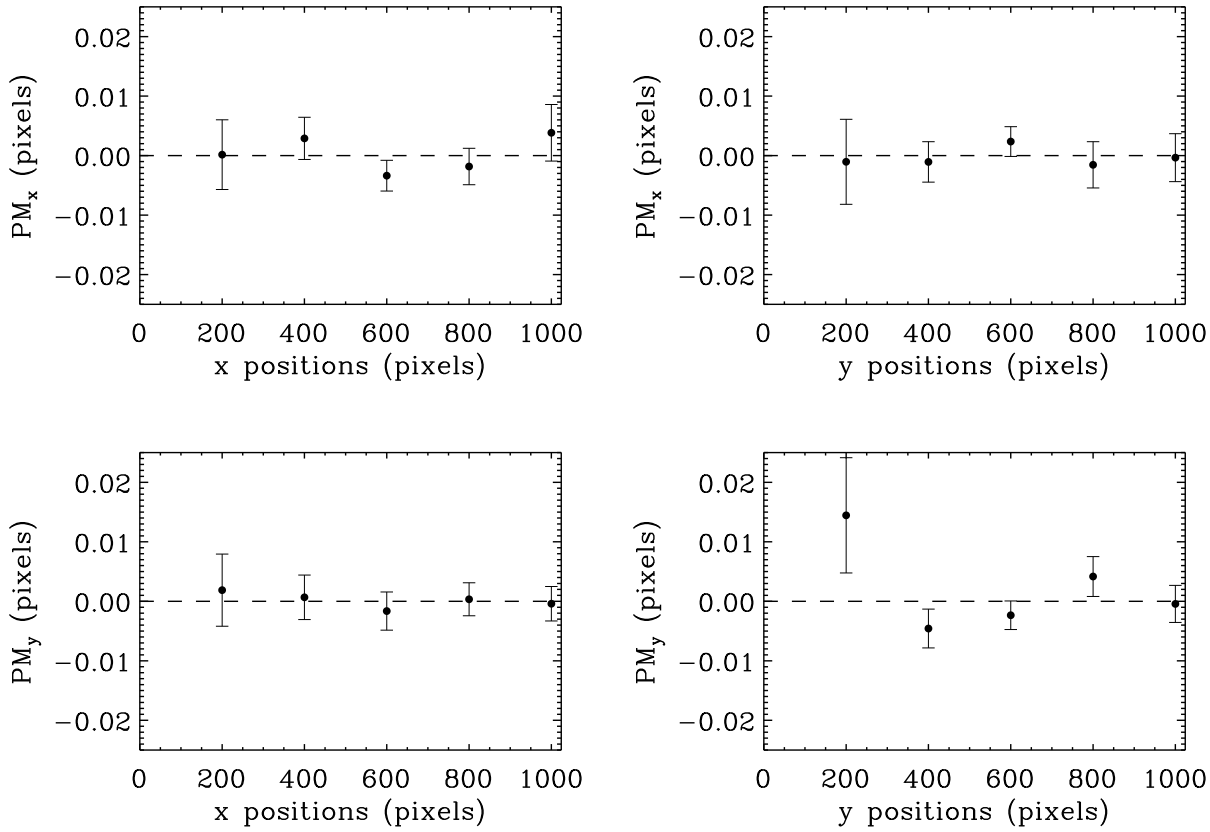

Fig. 6.— Average PMs of the stars in the masterlist that have PM and δPM < 0.1 pixels versus chip location. The PMs of the stars have been binned for every 200 pixels and then averaged.

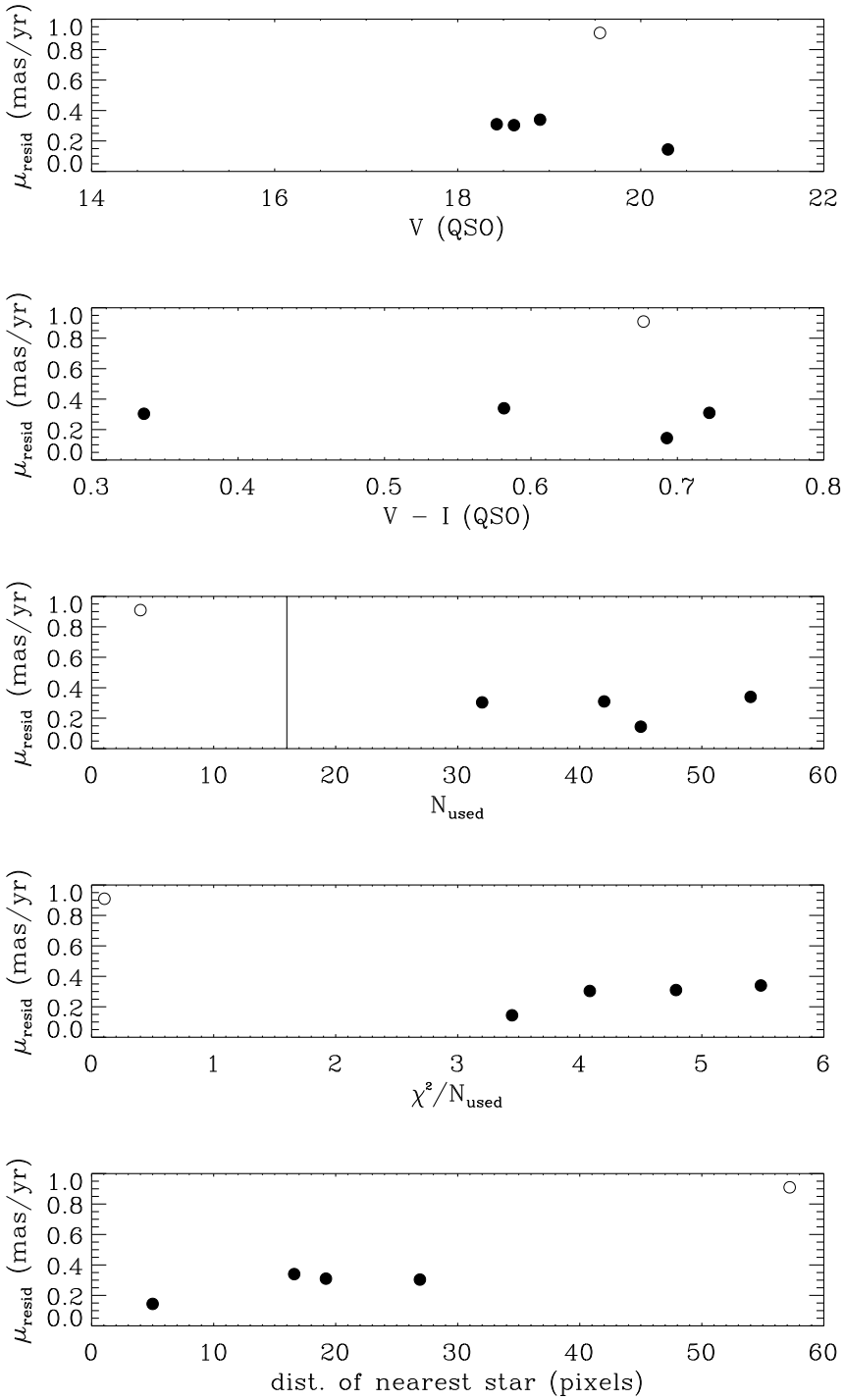

Fig. 7.— Plots of $\mu_{\rm resid}$ as a function of QSO V magnitude, $V-I$ color, $N_{\rm used}$, $\chi^2/N_{\rm used}$ and distance to the nearest neighboring star. We used the same criteria here as in Paper I, retaining only those fields with $N_{\rm used} > 16$ and $\chi^2/N_{\rm used} < 15$ (vertical lines) in our final sample (closed circles). The field that is rejected on the basis of these cuts (S4) is shown with an open circle in each panel.

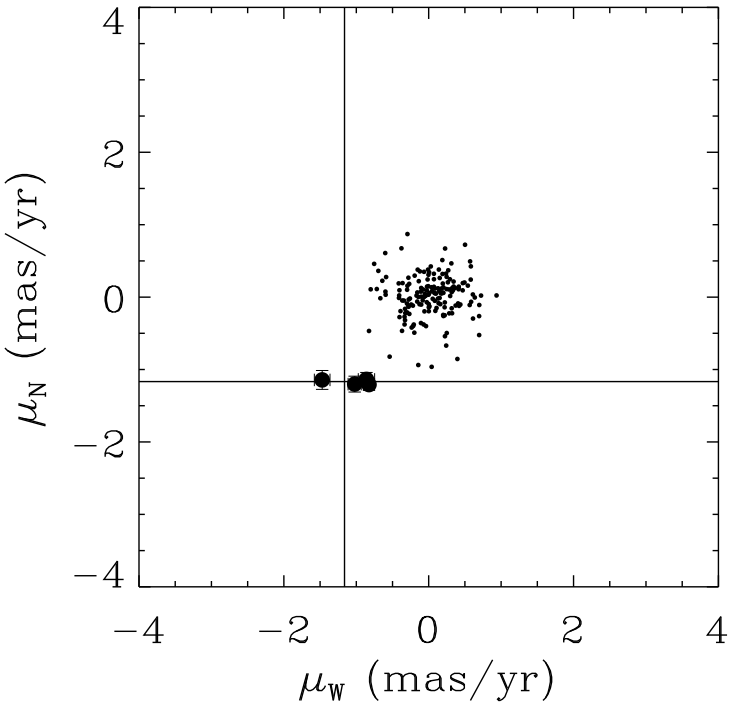

Fig. 8.— The observed PM (μ_W, μ_N) for the 4 QSO fields (i.e., -1 × the observed reflex motion of the QSO; columns 5 & 6 of Table 2) that pass all our criteria. The residual PMs of the SMC stars in the fields are plotted with open circles. The reflex motions of the QSOs clearly separate from the star motions. The straight lines mark the weighted average of the 4 fields, as listed in equation (1).

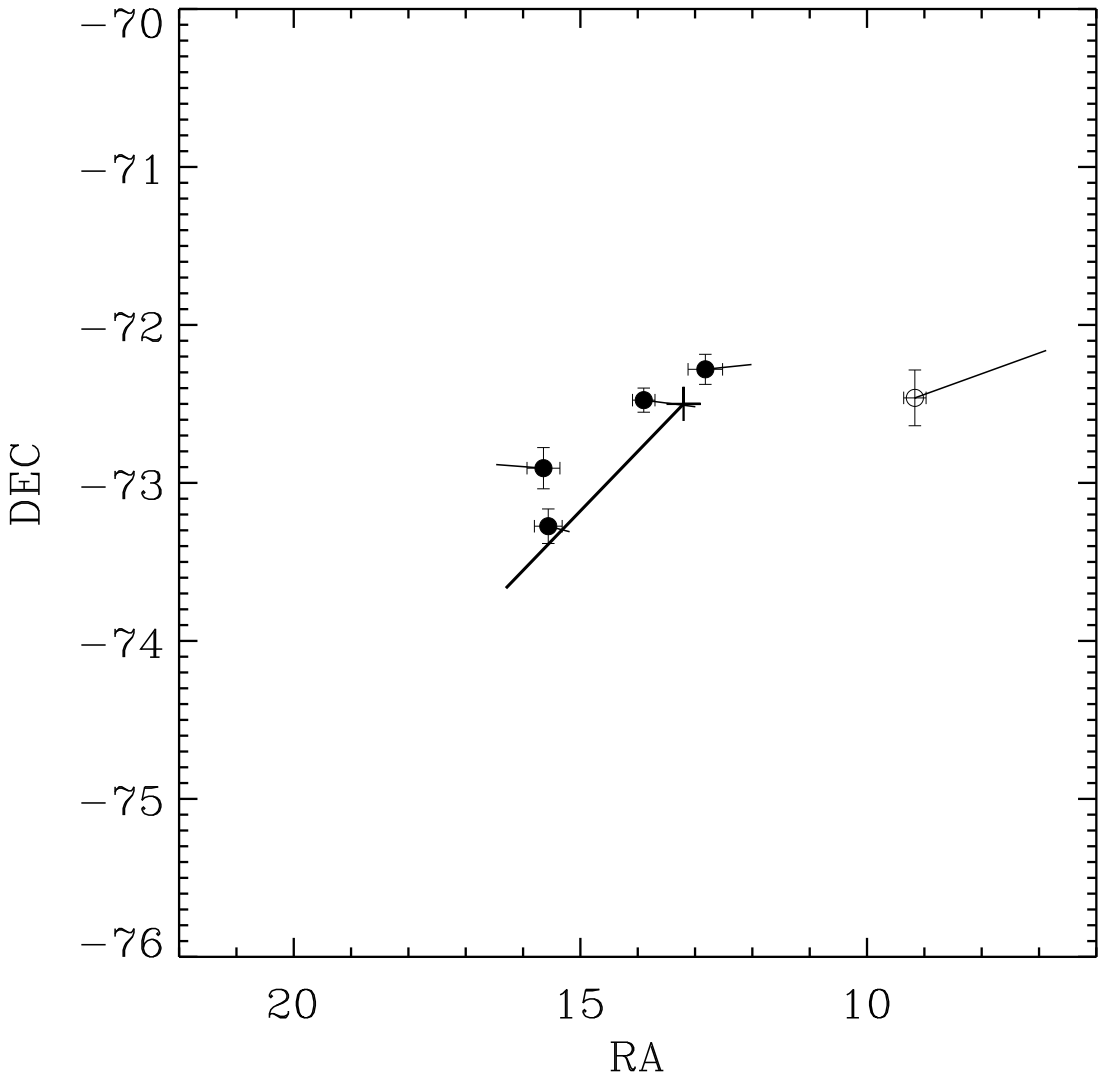

Fig. 9.— Circles show the positions of the QSO fields. The field that is rejected (from our final SMC PM estimate) is shown with an open circle and the 4 remaining fields are shown with filled circles. The error bars for each field are plotted as well. The vectors at these circles show the residuals between the PM estimates derived from the data for these fields and the adopted weighted average. The latter is given in equation (1) and is shown by the bold solid vector that is anchored by a plus sign.

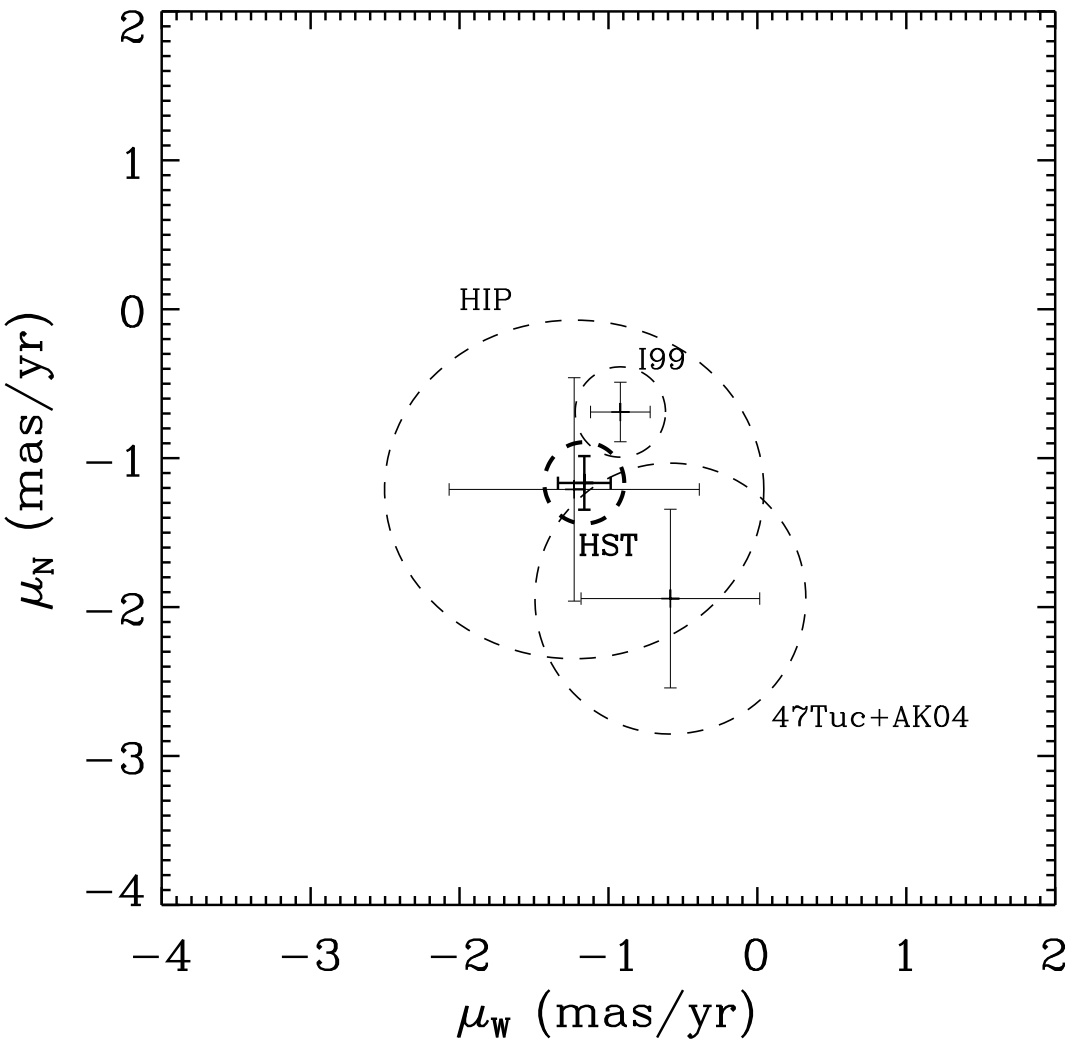

Fig. 10.— Plot of the (μ_W, μ_N)-plane spanned by the proper motion of the SMC from various studies. Dashed ellipses indicate the corresponding 68.3% confidence regions. The label HIP stands for the Kroupa & Bastian (1997) Hipparcos study, I99 for the measurement quoted in Irwin (1999), 47Tuc+AK04 for the value obtained by combining the Freire et al. (2003) and AK04 studies, and HST for this study.

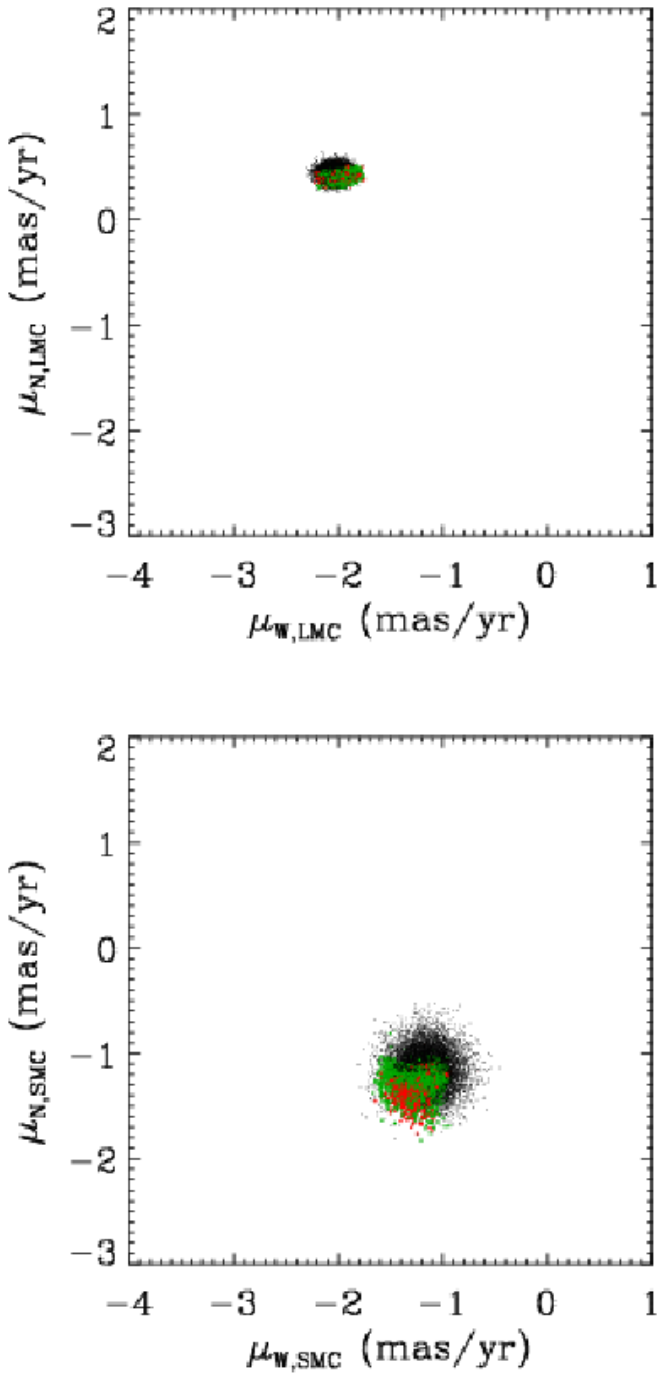

Fig. 11.— The past duration of the bound state of the Magellanic Clouds shown in the (μ_W, μ_N)-plane. The top panel shows the 10,000 initial proper motions drawn at random from the error ellipse of the LMC and the bottom panel shows the corresponding proper motions drawn from the error ellipse of the SMC. The duration of the bound state is represented by different colors, black for < 1 Gyr, green for between 1 & 5 Gyr and red for > 5 Gyr.

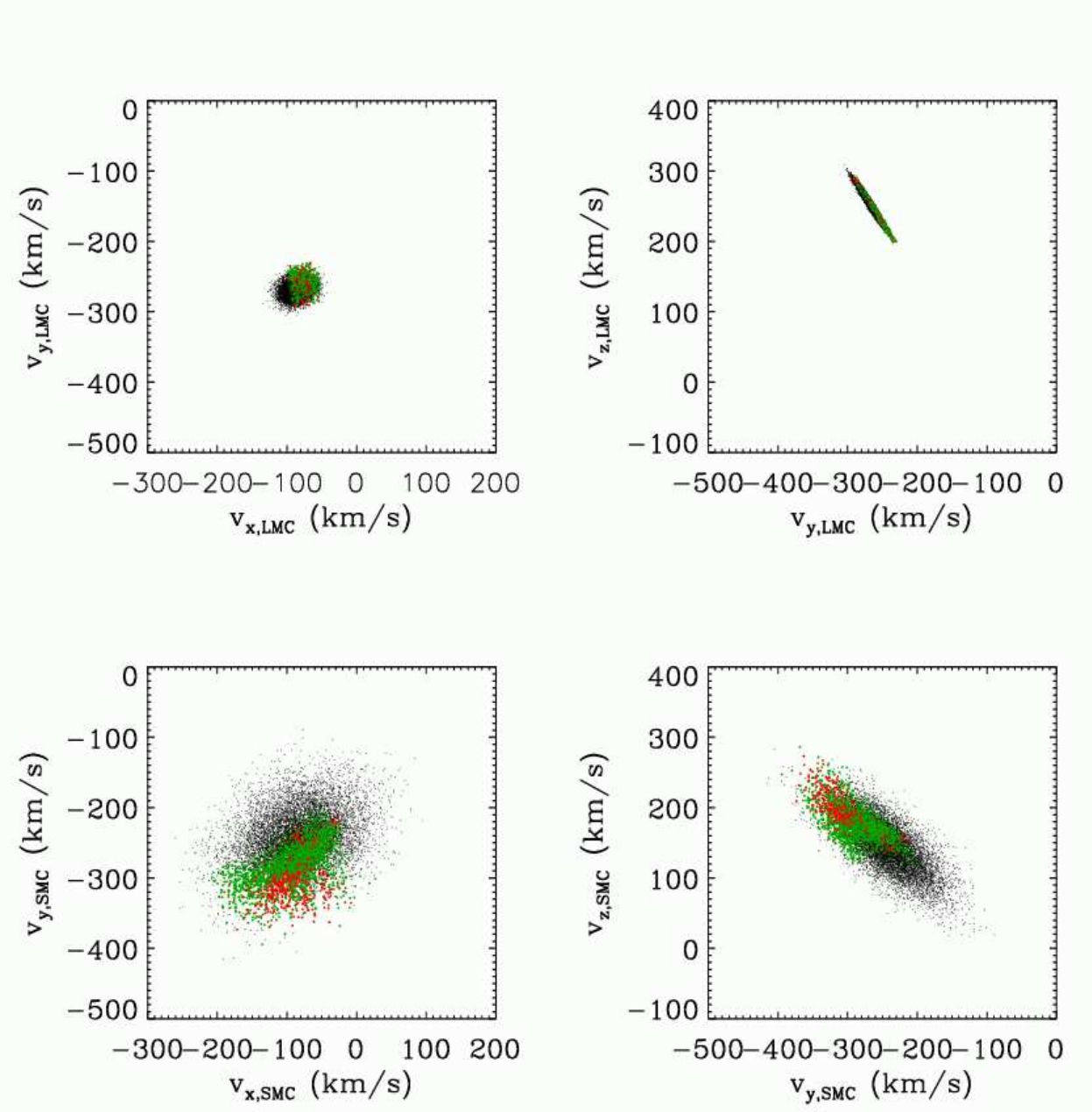

Fig. 12.— The past duration of the bound state of the Magellanic Clouds shown in Galactocentric velocity space. The top panel shows the initial velocities calculated from the proper motion error ellipse of the LMC and the bottom panel shows the same for the SMC. The duration of the bound state is represented by different colors, black for < 1 Gyr, green for between 1 & 5 Gyr and red for > 5 Gyr.

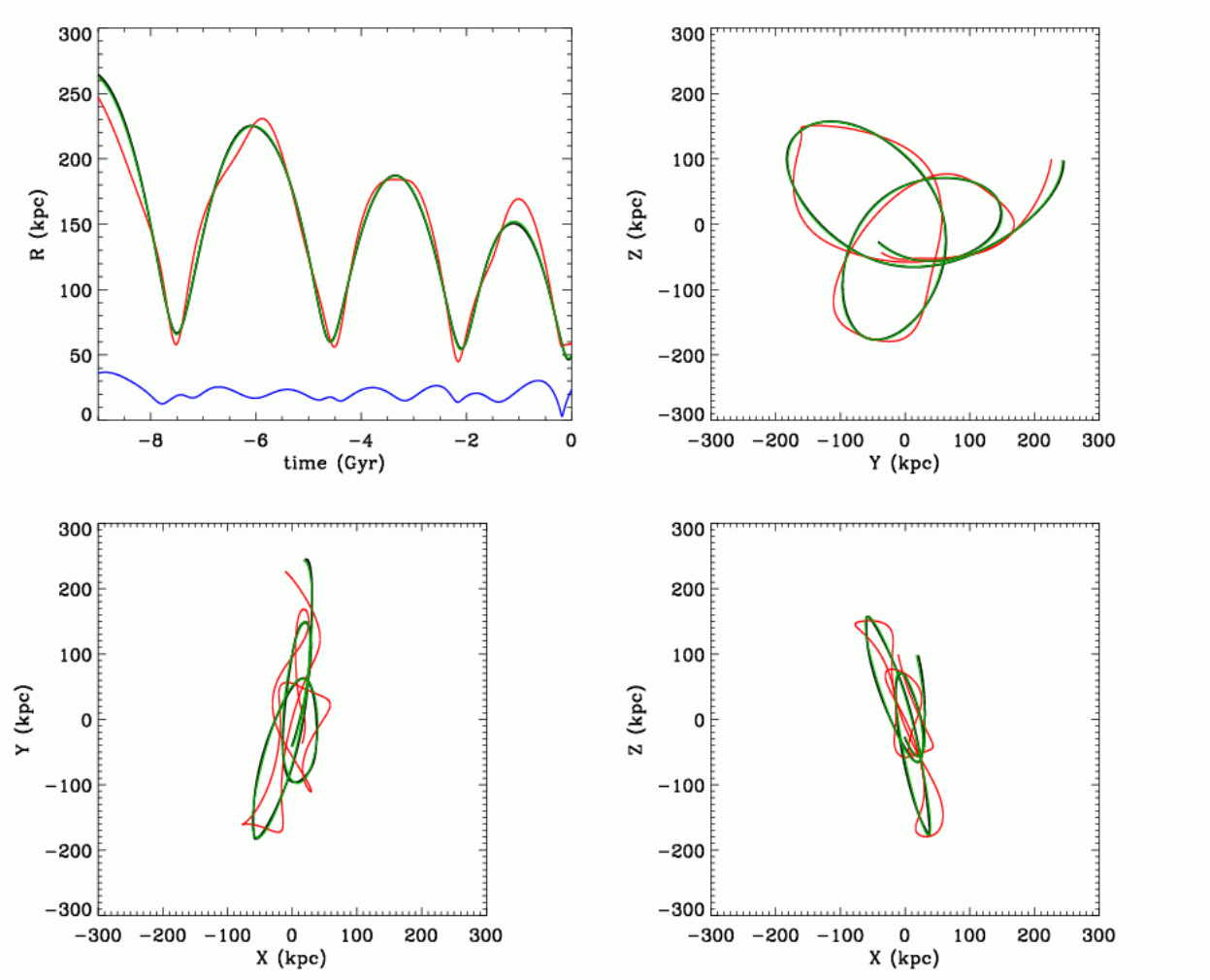

Fig. 13.— A representative bound orbit from our simulations. Black shows the Galactocentric distance of the LMC, red shows Galactocentric distance for the SMC and green for the center of mass of the two Clouds. The blue line shows the distance between the Clouds.

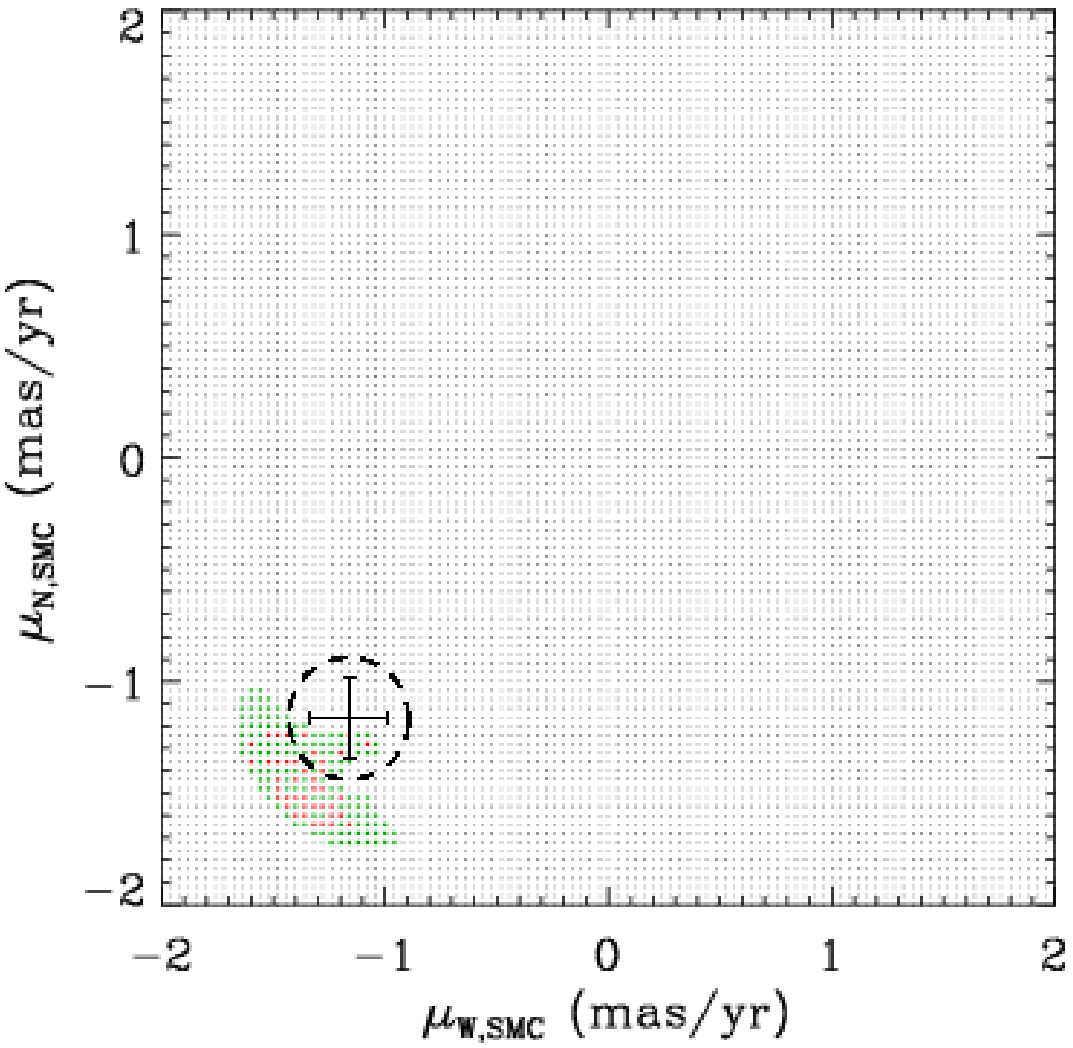

Fig. 14.— The past duration of the bound state of the Magellanic Clouds as a function of the SMC's current proper motion. The length of the bound state is represented by different colors, black for < 1 Gyr, green for between 1 & 5 Gyr and red for > 5 Gyr. The data point with error bars shows our measurement of the SMC's proper motion. The dashed ellipse is the corresponding 68.3% confidence region.

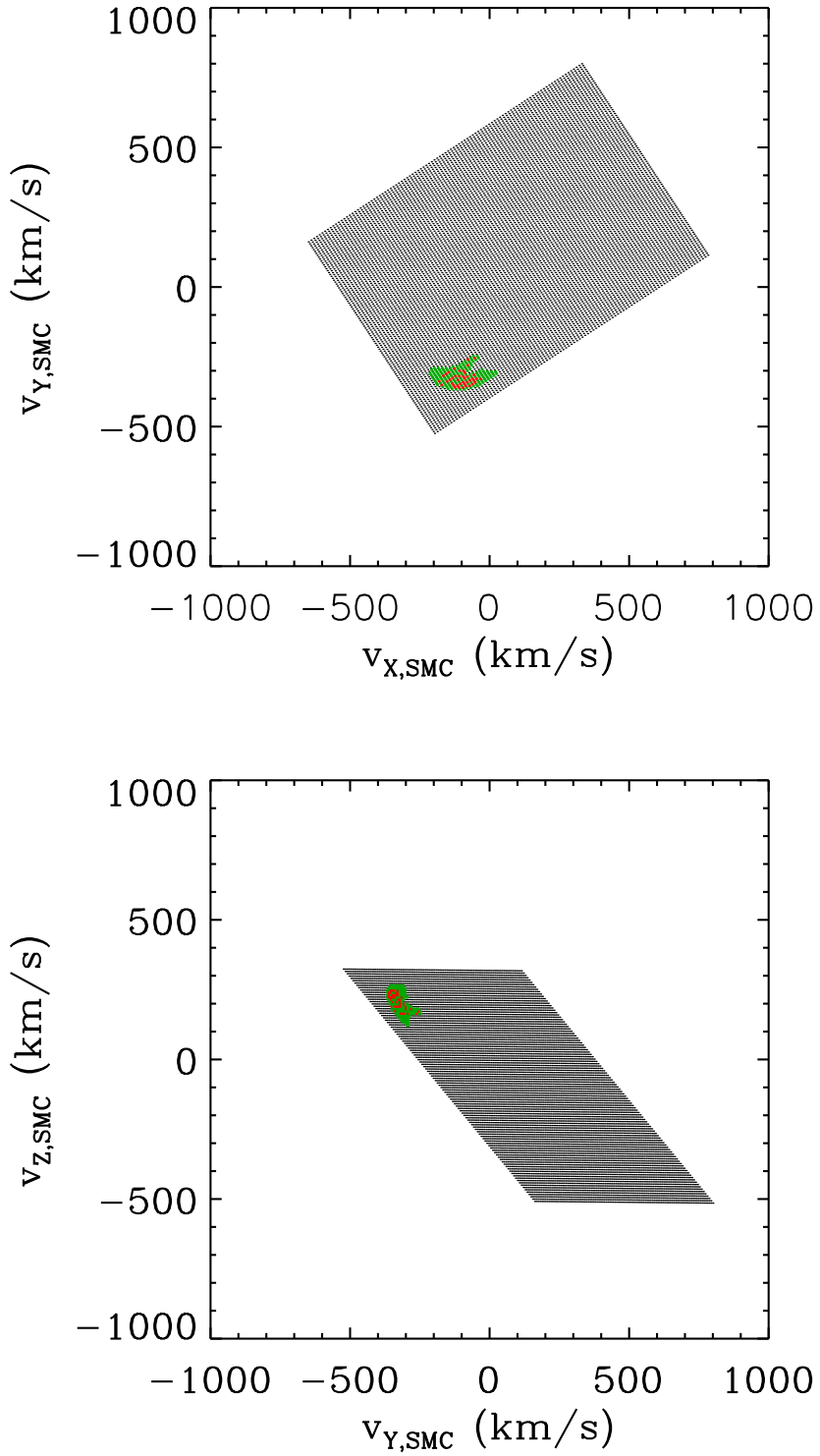

Fig. 15.— The past duration of the bound state of the Magellanic Clouds as a function of the SMC's current Galactocentric velocity. The length of the bound state is represented by different colors, black for < 1 Gyr, green for between 1 & 5 Gyr and red for > 5 Gyr.